**Atmospheric
Chemistry
and Physics**
Discussions

Open Access

Aerosol properties, source identification, and cloud processing in orographic clouds measured by single particle mass spectrometry on a Central European mountain site during HCCT-2010

A. Roth[1], J. Schneider[1], T. Klimach[1], S. Mertes[2], D. van Pinxteren[2],
H. Herrmann[2], and S. Borrmann[1,3]

[1]Particle Chemistry Department, Max Planck Institute for Chemistry, Hahn-Meitner-Weg 1, 55128 Mainz, Germany
[2]Leibniz Institute for Tropospheric Research (TROPOS), 04318 Leipzig, Germany
[3]Institute for Physics of the Atmosphere, Johann-Joachim-Becherweg 21, University of Mainz, 55128 Mainz, Germany

Correspondence to: J. Schneider (johannes.schneider@mpic.de)

Discussion Paper | Discussion Paper | Discussion Paper | Discussion Paper

ACPD

15, 24419–24472, 2015

Aerosol properties, source identification, and cloud processing

A. Roth et al.

Title Page

Abstract | Introduction

Conclusions | References

Tables | Figures

◀ | ▶▶

◀ | ▶

Back | Close

Full Screen / Esc

Printer-friendly Version

Interactive Discussion

Abstract

Cloud residues and out-of-cloud aerosol particles with diameters between 150 and 900 nm have been analysed by on-line single particle aerosol mass spectrometry during the six-week study HCCT-2010 in September/October 2010. The measurement location was the mountain Schmücke (937 m a.s.l.) in Central Germany. More than 170 000 bipolar mass spectra from out-of-cloud aerosol particles and more than 14 000 bipolar mass spectra from cloud residual particles were obtained and were classified using a fuzzy c-means clustering algorithm. Analysis of the uncertainty of the sorting algorithm was conducted on a subset of the data by comparing the clustering output with particle-by-particle inspection and classification by the operator. This analysis yielded a false classification probability between 13 and 48 %. Additionally, particle types were identified by specific marker ions.

The results from the ambient aerosol analysis show that 63 % of the analysed particles belong to clusters indicating a diurnal variation, suggesting that local or regional sources dominate the aerosol, especially for particles containing soot and biomass burning particles. In the cloud residues the relative percentage of large soot-containing particles and particles containing amines was found to be increased compared to the out-of-cloud aerosol, while in general organic particles were less abundant in the cloud residues. In the case of amines this can be explained by the high solubility of the amines, while the large soot-containing particles were found to be internally mixed with inorganics, which explains their activation as cloud condensation nuclei. Furthermore, the results show that during cloud processing, both sulphate and nitrate are added to the residual particles, thereby changing the mixing state and increasing the fraction of particles with nitrate and/or sulphate. This is expected to lead to higher hygroscopicity after cloud evaporation, and therefore to an increase of the particles' ability to act as cloud condensation nuclei after their cloud passage.

1 Introduction

The interaction of aerosol particles and cloud droplets has several aspects: on the one hand, the presence of a cloud condensation nucleus (CCN) is an essential prerequisite for the formation of a cloud droplet, and the size and chemical composition of the aerosol particle determines whether a particle acts at a certain temperature and supersaturation as a CCN or not (e.g., Dusek et al., 2006; Gunthe et al., 2009). On the other hand, cloud processing alters the chemical composition of the cloud droplet such that after evaporation of the cloud droplet the remaining aerosol particle is of different composition than the original CCN. The uptake of nitric acid in the aqueous phase of cloud droplets has been observed (Hayden et al., 2008), but also sulphate is known to be produced by oxidation of SO_2 in the cloud phase, either by reaction with O_3 (Bower et al., 1991), H_2O_2 (Bower et al., 1997; Laj et al., 1997a) or by transition metal induced oxidation (Harris et al., 2014). Both effects lead to a higher content of water soluble inorganic material in the aerosol which is expected to enhance the cloud formation potential of the particles.

Cloud particle sampling and separation from the not activated interstitial aerosol can be achieved by applying a counterflow virtual impactor (CVI, Ogren et al., 1985; Mertes et al., 2005b; Wendisch and Brenguier, 2013). This technique has been coupled with on-line aerosol mass spectrometry before, such that the composition of the cloud droplet residues during individual clouds can be measured with high time resolution (Drewnick et al., 2007; Allan et al., 2008; Hayden et al., 2008). The use of single particle mass spectrometry for single cloud residual particle analysis (e.g., Gieray et al., 1997; Kamphus et al., 2010; Pratt et al., 2010; Zelenyuk et al., 2010), gives not only the composition of the bulk residues but also the mixing state of the cloud residues. Comparison with the aerosol observed shortly before cloud formation can give information on the possible addition of chemical compounds in the cloud phase and thereby evidence for cloud processing.

Several previous hill cap cloud experiments – considering the clouds as "stationary flow processors" – have been conducted and results have been reported in the literature. One of these is the FEBUKO experiment (Herrmann et al., 2005) which took place at the same field site as the HCCT-2010 experiment reported here. The results from FEBUKO have shown a measurable increase of sulphate and ammonium, but only in 2 of 3 investigated cases, and only in the smallest particle size range (up to 140 nm; Brüggemann et al., 2005). The mass production in the clouds was about 5 % of upwind aerosol mass (in a size range between 60 and 300 nm, Mertes et al., 2005a). Tilgner et al. (2005) found from model calculations for the same experiment that the mass increase is mainly due to HNO_3 uptake and only to a lesser degree due to SO_2 oxidation.

The Kleiner Feldberg Cloud Experiment (Fuzzi et al., 1994; Wobrock et al., 1994) was conducted in 1990. Off-line single particle analyses of cloud residues sampled via a counterflow virtual impactor during this experiment are reported by Hallberg et al. (1994). It could be shown that the majority of cloud residues contained soluble compounds whereas insoluble particles remained in the interstitial air. Fuzzi et al. (1994) report from the Feldberg Cloud Experiment that a general lack of gaseous NH_3 was observed in the cloud systems. So clouds were acidic either by uptake of HNO_3 or by oxidation of NO_2 via O_3 in the aqueous phase. SO_2 oxidation in these clouds was inhibited by a lack of H_2O_2 and the low pH-values being not an explanation for the verified sulphate concentration in the cloud water.

During the Great Dun Fell experiment which took place in 1993 an increased sulphate concentration of the aerosol was observed after cloud passing (Laj et al., 1997b). Thereby also the ammonium concentration increased based on the neutralization reaction with ammonia. The increased sulphate concentration could be attributed mainly to SO_2 oxidation by H_2O_2 in the cloud water and to a lesser extent by O_3 (Bower et al., 1997; Laj et al., 1997a). Furthermore, even though the concentrations of iron and copper were low, an influence of these elements on formation and depletion of photo-oxidants could be recognized (Sedlak et al., 1997).

Here we report the results obtained from individual particle chemical analysis by on-line single particle laser ablation mass spectrometry during the hill cloud experiment HCCT-2010, which was conducted on the mountain site Schmücke in September and October 2010 in Central Germany. The analysis includes cloud residual particles that
5 were sampled from the cloud using a CVI and aerosol particles that were measured during cloud-free periods.

2 Experiments and data evaluation procedures

2.1 Measurement site and instrumentation

The Hill Cap Cloud Thuringia (HCCT) 2010 experiment took place between 13
10 September 2010 and 25 October 2010, at the mountain ridge "Thüringer Wald" in Central Germany. The same measurement sites were used as during two previous experiments (FEBUKO 2001 and 2002; Herrmann et al., 2005): (1) an upwind site (Goldlauter, 605 m a.s.l., $10°45'20''$ E, $50°38'28''$ N), (2) a summit site (Schmücke, 937 m a.s.l., $10°46'15''$ E, $50°39'19''$ N), and (3) a downwind site
15 (Gehlberg, 732 m a.s.l., $10°47'32''$ E, $50°40'21''$ N). At the summit site Schmücke, two particle inlets were installed in south-westerly direction in separate windows at the height of 15 m of a 3-story building that hosts a field station of the German Environ-mental Protection Agency (Umweltbundesamt). The aerosol inlet was used to sample aerosol particles with aerodynamic diameters (d_{aero}) smaller than 5 µm under cloud
20 free conditions. During cloudy periods the CVI (Mertes et al., 2005b) was additionally deployed to sample cloud droplets with diameters larger than 5 µm. The single particle aerosol mass spectrometer ALABAMA (Aircraft-based Laser Ablation Aerosol Mass Spectrometer) was operated while manually alternating between these two inlets. In-terstitial aerosol was not detected by the ALABAMA and is therefore not considered in
25 this study.

A detailed description of the mass spectrometer ALABAMA can be found in Brands et al. (2011).The particles enter the vacuum chamber via a Liu-type aerodynamic lens (Liu et al., 1995b, a) and are focused to a narrow particle beam. Due to the pressure drop the particles are accelerated when exiting the aerodynamic lens. The final particle velocity depends on their size, shape and density. The particles are detected by the scattered light of two orthogonal continuous wave Nd:VO$_4$ laser beams (λ = 532 nm). The optical detection of the particles limits the particle size range for smaller particles to about 150 - 200 nm. The particle size given as the vacuum aerodynamic diameter (d_{va}) can be derived from the time difference between the two scattering signals by means of calibration with particles of known size. In addition the time difference is used to calculate the time at which a particle will arrive at the ionization region of the mass spectrometer. There the particle is evaporated and ionized in one step by laser ablation with a pulsed Nd:YAG laser (λ = 266 nm). The resulting positive and negative ions are detected by a bipolar time-of-flight mass spectrometer. The laser ablation method is a qualitative method, such that it is not possible to relate the peak height to a mass concentration of a certain compound (e.g., Middlebrook et al., 2003).

Figure 1 shows the measurement set-up and additionally operated instruments at the summit site Schmücke. Besides the ALABAMA, an optical particle counter (OPC, Grimm, model 1.109, time resolution 6 s) as well as an Compact Time-of-Flight Aerosol Mass Spectrometer (C-ToF-AMS, Aerodyne Research Inc., Drewnick et al., 2005) were run simultaneously. Furthermore a High Resolution Time-of-Flight AMS (HR-ToF-AMS, Aerodyne Research Inc., DeCarlo et al., 2006) and a multi-angle absorption photome-ter (MAAP, Thermo Scientific, model 5012, time resolution 1 min) were operated con-tinuously at the aerosol inlet. The MAAP determines the mass concentration of equiv-alent black carbon (EBC, Petzold et al., 2013) based on the absorption of particles sampled on a filter. The results from the C-ToF-AMS and HR-ToF-AMS measurements are presented in an accompanying paper (Schneider et al., 2015). Outside of the build-ing, a particle volume monitor (PVM, Gerber Scientific Inc., model 100, time resolution 1 min) for investigation of the liquid water content (LWC) and a weather station (Davis

Vantage Pro) for meteorological parameters were installed. Additionally, Caltech active strand cloud water collectors (one stage, three stage, and five stage) were mounted. The pH-value as well as the content of organic compounds of cloud water were analysed by off-line methods at TROPOS. Furthermore, aliphatic amines were analysed from filtrated cloud water samples (0.45 µm syringe filters, Acrodisc 13, Pall, Dreieich, Germany) using an ion chromatography method adopted from Facchini et al. (2008). Details of the method are given elsewhere (van Pinxteren et al., 2015).

2.2 Definition of Full Cloud Events (FCE)

During the campaign a measurement period was considered as a "full cloud event" (FCE) when the air masses passed all three measurement sites and when the criteria described in Tilgner et al. (2014) were fulfilled. During HCCT-2010, 14 FCEs were identified (Tilgner et al., 2014) and evaluated (Table 1). In this study we present the data from all cloud residue measurements behind the CVI, but additionally the official FCEs are analysed separately, thereby facilitating comparison with other data from HCCT-2010. FCEs showing insufficient number of mass spectra for statistical evaluations (FCE2.1, FCE4.1, FCE5.1 and FCE 26.2) are not considered in the following data analysis.

2.3 Back trajectory calculation

Back trajectories for the air masses encountered during HCCT-2010 were calculated using HYSPLIT (Hybrid Single-Particle Lagrangian Integrated Trajectory, Draxler and Rolph, 2012). The air mass origin was determined 96 h before arriving at Mt. Schmücke with a time resolution of 1 h. The coordinates of the Schmücke at a height of 500 m above the ground were used as endpoint in the model. 500 m were chosen because the model orography can not resolve a small scale mountain range like the Thüringer Wald with sufficient detail. The back trajectories for the whole HCCT-2010 campaign

can be found in the Supplement (Fig. S1). Back trajectories for the FCE are discussed in Sect. 3.3.

2.4 Analysis of single particle mass spectra

During the whole HCCT-2010 campaign the ALABAMA sampled over 286 000 single particle mass spectra. The mass spectra were distinguished between out-of-cloud aerosol and cloud residual particles according to the inlets and the LWC. For the analysis of out-of-cloud aerosol only measurement periods with an LWC $< 0.05\,\mathrm{g\,m^{-3}}$ were considered (402 h) while data sampled behind the CVI were only examined for an LWC $> 0.1\,\mathrm{g\,m^{-3}}$ (228, 106 h during FCEs). Upon inspection of the data set, a certain number of mass spectra were found to contain ions of only one polarity. The appearance of such mono polar mass spectra was also observed in other single particle mass spectrometer measurements (Bein et al., 2005; Sodeman et al., 2005; Shields et al., 2007; Pratt et al., 2010) resulting either from technical issues (e.g. tuning of high voltages) or from ion formation of only one polarity (Sodeman et al., 2005). Negative ion mass spectra provide better information on secondary organic and inorganic compounds (nitrate and sulphate) and thereby also on the mixing state of the particles. However, in order to constrain the analysis to a consistent data set, monopolar mass spectra were excluded and only mass spectra of both polarities were considered for the data analysis presented here. Out of the remaining 177 752 bipolar single particle mass spectra 164 595 were obtained while sampling out-of-cloud aerosol and 13 157 while sampling cloud residues (out of these 4 400 were obtained during FCEs).

2.4.1 Clustering by fuzzy c-means algorithm

The analysis method that is widely used and has become a standard method for single particle mass spectra data is the clustering of the data set by similarities of the mass spectra (e.g., Hinz et al., 1999; Silva and Prather, 2000; Murphy et al., 2003; Hinz et al., 2006; Zelenyuk et al., 2006; Hinz and Spengler, 2007; Zelenyuk et al., 2008;

Zhao et al., 2008; Dall'Osto et al., 2009). The analysis presented here was conducted using the software tool CRISP (version 1.127, 64 bit) that was recently developed at MPIC (Klimach, 2012). It is based on the programming software IGOR Pro (version 6.3, WaveMetrics). CRISP facilitates processing and management of large data sets. Data processing includes mass calibration of the time-of-flight spectra, peak area integration, and either automated clustering by one of the implemented algorithms (k-means or fuzzy c-means), or manual clustering by inspection of every mass spectrum. Furthermore particle spectra can be selected by specified criteria or according to additional external data sets. Here the clustering was done using the fuzzy c-means algorithm (Bezdek, 1981; Bezdek et al., 1984; Hinz et al., 1999). All 177 752 bipolar mass spectra were first pre-processed separately by calculating the square root of the peak intensity for every peak in order to reduce peak intensity differences. Afterwards the mass spectra were normalized (positive and negative polarities separately) to the sum of the peak intensities. After concatenation of both polarities the entire mass spectrum was normalized again. In the algorithm the starting reference mass spectra for the clustering are chosen as follows: the first mass spectrum of the data set is chosen as the first reference. Hereupon the distance between the first reference and all further mass spectra is calculated sequentially. If the Pearson correlation coefficient between the reference and the actual mass spectrum is smaller than a threshold (chosen here: 0.8), the latter is regarded as being significantly different from the first reference spectrum and is added as a further start cluster reference. This procedure is repeated until the desired number of start clusters (here: 200) is obtained. The membership coefficient m_{ik} for every particle spectrum i to a cluster reference k is calculated by:

$$m_{ik} = \frac{1}{\sum_{j=1}^{c} \left(\frac{d_{ik}}{d_{ij}}\right)^{\frac{2}{f-1}}} \tag{1}$$

with the number of clusters c, the "fuzzifier" f and the distance d_{ij} between mass spectrum i and reference j. The sum of all membership coefficients equals 1. The

fuzzifier ($1 \leq f \leq \infty$, originally introduced as "weighting exponent" by Bezdek, 1981) represents the fuzziness (blurring, defocusing) of the classification. The fuzzifier value of 1.7 applied here was chosen empirically on the basis of test data sets with known particle types and particle numbers. The distance d_{ij} is calculated here based on the Pearson correlation coefficient r_{ij} ($0 \leq r_{ij} \leq 1$) between the particle spectrum i and the cluster reference j via:

$$d_{ij} = 1 - r_{ij} \tag{2}$$

Every mass spectrum is compared to the start clusters, calculating correlation coefficient, distance and membership coefficient. Afterwards a mean mass spectrum of every cluster is calculated under consideration of the membership coefficients. The new mean cluster spectrum serves as reference for the following run. Again correlation, distance and memberships are calculated for every mass spectrum to the new cluster references. This procedure is repeated until the membership difference of two consecutive iterations is smaller than a termination threshold (here: 10^{-4}). Now every mass spectrum is assigned to that cluster for which the Pearson correlation coefficient r_{ij} is highest, but only if r_{ij} is larger than a certain threshold (here: 0.7). Mass spectra showing smaller correlation coefficients than this threshold are sorted out and assigned to an additional cluster ("others").

The clustering of the current data set resulted in 159 clusters. This number is smaller than the starting value of 200 clusters, confirming that the chosen number of 200 starting cluster was large enough and that no particle types that significantly differ from the others were missed by the algorithm. About 9 % of all mass spectra were sorted out being represented by the fraction "others". According to the fragmentation pattern considering characteristic peaks for certain particle types, their combination (e.g. Hinz et al., 1999; Trimborn et al., 2002; Vogt et al., 2003; Dall'Osto and Harrison, 2006; Pratt and Prather, 2010; Corbin et al., 2012) and relative peak intensities, every cluster was assigned manually to a certain particle type. Afterwards the number of obtained clusters was reduced by combining clusters of the same particle type, if two mean cluster

spectra j and k showed a Pearson correlation coefficient r_{jk} larger than 0.7. In this way 65 cluster types remained which were further grouped into 19 different fragmentation types (plus "others") representing 11 distinguished particle types (plus "others"), according to the criteria given in Table 3 (A-K). All cluster mean mass spectra as well as further details on the separation of different clusters are shown in the Supplement (Figs. S2–S5; Table S1). Further particle types were determined by searching for specific marker peaks, see Sect. 2.4.3.

2.4.2 Uncertainties of clustering by the fuzzy c-means algorithm

By manual inspection of the cluster algorithm results it was found that occasionally mass spectra were classified falsely by the algorithm, depending on cluster number and particle type. To take into account uncertainties of the resulting particle type fractions, the uncertainties were estimated by means of a reduced, representative data set of the HCCT-2010 campaign. For this, 1377 single particle mass spectra were clustered by fuzzy c-means using the same parameters as described above. The resulting clusters were assigned to particle types based on their averaged mass spectrum. Afterwards the individual mass spectra of every particle type were reviewed manually. For example, 274 particle spectra were sorted into the particle type "org, K". The number of mass spectra being assigned falsely to the considered particle type was determined ($\Delta_{\text{false positive}}$). In case of "org, K", 51 mass spectra of this particle type belonged to a different particle type. The number of mass spectra being classified falsely to another particle type was also determined ($\Delta_{\text{false negative}}$). In order to do this, all other clusters were inspected and the number of mass spectra belonging actual to "org, K" was counted. In this example, 43 mass spectra of the particle type "org, K" were assigned to clusters of other particle types by the algorithm. Since both false classifications are not dependent on each other, we chose to apply Gaussian error propagation for the determined uncertainty of a particle type ($\Delta_{\text{particle type}}$):

$$\Delta_{\text{particle type}} = \sqrt{\Delta_{\text{false positive}}^2 + \Delta_{\text{false negative}}^2}. \tag{3}$$

In case of "org, K", $\Delta_{\text{particle type}} = 67$, meaning that the error is about 24 % of the absolute number of mass spectra of this cluster. Due to the fact that a reduced data set was applied, not all particle types were included, because no particle of the type "mineral dust" and "Ca" were present in the test data set. The uncertainty for the particle type "Ca" was therefore estimated by averaging the uncertainties of the other particles types, while the particle type "mineral dust" was further refined by the marker method and the uncertainty was inferred as explained in Sect. 2.4.3. Table 2 shows the details of the test data set along with the resulting uncertainties for the different particle types. In this test case, a total of 16 % of all mass spectra were assigned to a wrong particle type. In relation to the absolute number of each particle type, $\Delta_{\text{particle type}}$ ranges 13 and 50 %. The largest uncertainties are found for the particle types "diesel exhaust" (50 %), "amines" (35 %), "soot and org" (31 %) and "K" (30 %). The large error bar of the fraction "others" can be explained by the exclusion of mass spectra that would have been assigned manually to an existing particle type. The determined uncertainties were adopted for the clustering of the total data set.

2.4.3 Particle type identification by marker peaks

In addition to the clustering method that compares the whole mass spectra of the individual particles, it is also useful to search for certain marker peaks, especially in cases when these peaks are of small intensity such that they do not influence the correlation of two mass spectra and therefor do not show up in the clustering results. A typical example would be looking for metals (e.g., lead) or rarely appearing particle types (Dall'Osto et al., 2004; Tolocka et al., 2004; Snyder et al., 2009). By the marker method it was possible to identify two different particle types characterized by the abundance of iron, namely "mineral dust" and "Fe, V" (iron internally mixed with vanadium). Indicators for mineral dust are besides Fe^+ also Na^+ (m/z 23) and K^+ (m/z 39) (Silva et al., 2000; Hinz et al., 2006; Dall'Osto et al., 2010), while Vanadium (V^+, m/z 51) originates rather from fuel combustion (Tolocka et al., 2004; Korn et al., 2007; Ault et al., 2010) and industrial sources like refineries (Dall'Osto et al., 2004; Ault et al., 2009) than from

mineral dust. Details on the classification of iron containing particles can be found in the Supplement (Sect. 3, Fig. S6).

The method is also suitable for investigating the particle mixing state when looking at the abundance of, e.g., nitrate and sulphate independent of the particle type. Uncertainties for particle types derived by the marker method were estimated using counting statistics.

2.4.4 Combined analysis using clustering and marker peaks

In order to optimize the data analysis and as a consequence of the two preceding sections, we chose to apply a combined method of clustering and marker peaks: after the clustering, the fraction "others" has been additionally investigated by marker peaks of lead, nickel, vanadium, and iron. Also the particle type characterized by iron inferred from the clustering method was analysed further using the marker peak method, resulting in two particle types: one interpreted as mineral dust and the other consisting of iron internally mixed with vanadium ("Fe, V"), belonging probably to an industrial source. Using the combined method of clustering and marker peak analysis, a total of 14 particle types plus "others" were identified. A summary of the resulting particle types, the applied method and their characteristic signals for identification as well as the corresponding chemical composition in the mass spectra are listed in Table 3. Due to the fact that all particle types were internally mixed with secondary inorganic compounds like nitrate and sulphate, these compounds are not explicitly mentioned in the legend. The mean positive and negative mass spectra of the 14 particle types plus the averaged remaining mass spectra ("others") are shown in Fig. 2. An overview of all cluster types obtained by the clustering method can be found in the Supplement (Figs. S2–S5).

3 Results

3.1 Size resolved aerosol composition and identification of local sources

Figure 3 shows the size resolved particle composition for all particles (not separated for out-of-cloud aerosol and cloud residues). The relative fraction of all particles in the specific size class is given in order to eliminate the size dependent detection efficiency of the ALABAMA (Brands et al., 2011). The total number of analysed particles per size bin is given by the grey line. The maximum of the analysed particles lies in the size range between 500 and 550 nm, due to the best detection and ablation efficiency of the ALABAMA in this size range. The particle types shown in Fig. 3 refer only to the results obtained by the fuzzy c-means clustering, thus the particle types "Fe, V", "Ni", and "Pb" are contained in the type "others". The most abundant particle types are "org, K", "biomass burning" and "soot" (see also Table 4). The particle types "diesel exhaust" as well as "soot, org" only appear significantly at small vacuum aerodynamic diameters between 200 and 450 nm. This indicates that these particles were recently emitted and had no time grow by condensation or coagulation. In contrast, the particle types "org", "amines" and "soot", are observed only with diameters larger than 450 nm. This agrees with the observation that all analysed soot particles were internally mixed with nitrate and sulphate (see Sect. 3.4) and indicates that these soot particles were aged and have been processed and coated. Particles of the type "biomass burning" and "org, K" are found in all size classes, although the type "org, K" has a clear maximum between 400 and 500 nm.

Figure 4 shows the percentage of particles that were analysed during certain local wind directions at the Schmücke. The graph shows that about 50 % of all particles were detected when the wind was coming from south-western directions between 180 and 270° and about 25 % of the particles were detected when the wind came from north-east respectively east ($\sim$ 40–100°). The wind velocities are indicated by the colour code: wind velocities were higher during south-westerly winds (mainly between 10 and 30 km h^{-1}; red and blue), while during north-easterly wind directions the wind velocity

was mainly between 10 and 20 km h^{-1} (red). North-westerly and south-easterly wind directions were almost not observed at all at the measurement station.

   Several particle types show a distinct diurnal pattern, indicating a source with a specific emission pattern. The fact that the emission pattern is detectable at the measurement site suggests that the source is not too far away, such that the diurnal pattern is not smoothed by different air mass transport velocities and different wind directions. An example is shown in Fig. 5. The figure shows the complete time series for the particle type "diesel exhaust" (upper panel) and the averaged diurnal pattern (lower panel). The diurnal pattern shows the increased occurrence of particles of this type between 09:00 and 24:00 LT and a decrease of this particle type during the night. This indicates the contribution of traffic emissions from within one or two hours from the measurement site (local traffic typically starts around 07:00 LT in the morning). All clusters contained in each particle type were inspected for such a diurnal trend. From this the amount of particle influences by local or regional sources were obtained. Table 4 shows the relative abundance of the particle types during HCCT-2010 along with the percentage of clusters showing diurnal variations and those not showing a diurnal trend. In total, about 63 % of the analysed particles belong to clusters indicating a diurnal variation. This finding implies that the aerosol composition during HCCT-2010 is mainly influenced by local and regional sources.

3.2   Comparison of out-of-cloud aerosol and cloud residues

One of the main objectives of this study was the analysis of cloud residues and the comparison to the aerosol composition under cloud-free conditions. Figure 6 shows the average aerosol particle composition for all out-of-cloud aerosol particles and all cloud residues measured during HCCT-2010, not restricted to the full cloud events. It has to be noted that measurements of cloud residues and out-of-cloud aerosol can by definition not be made simultaneously, such that differences in the meteorological condition influences such a comparison. In the following we will compare the relative

abundance of the individual particle types between cloud residues and out-of-cloud aerosol.

3.2.1 Organic particle types

For both organic particle types ("org, K" and "org") the relative abundance in cloud residues is smaller than in the out-of-cloud aerosol. This observation may partly be in contradiction with previous measurements reported in the literature. For example, measurements of cloud residue composition by Drewnick et al. (2007) using an Aerodyne AMS reported increased organic mass fractions in cloud residues. However, these measurements are hard to compare because AMS data are based on average aerosol mass while the ALABAMA date are based on single particle type occurrence. Furthermore, Drewnick et al. (2007) did not consider refractory species in the aerosol composition and did not separate the organic mass into different subgroups. For example, in our study the particle types "soot" and "biomass burning" reveal a significant fraction of the aerosol composition (see below), and aerosol originating from biomass burning can be a significant fraction of the "organic" aerosol mass reported by the AMS (e.g., Lanz et al., 2010; Crippa et al., 2013, 2014). The AMS data from the HCCT-2010 campaign that are presented in a companion paper (Schneider et al., 2015) show a slightly lower scavenging efficiency for organics than for nitrate and sulphate. In-cloud scavenging of organic particles depends on the solubility of the organic compounds (Limbeck and Puxbaum, 2000). The slightly lower scavenging efficiency may therefore be explained by the lower solubility of hydrophobic organic compounds like aromatics whose fragments were frequently observed our single particle mass spectra ($C_4H_3^+$ (m/z 51), $C_6H_5^+$ (m/z 77), $C_9H_7^+$ (m/z 115), see mass spectrum "org, K_2" in Fig. S2).

3.2.2 Amine-containing particles

Several characteristic peaks for amines have been reported in the literature, the most common appear to be m/z 59 ((CH_3)$_3$N$^+$) and m/z 74 ((C_2H_5)$_2$NH$_2^+$) (Angelino et al.,

2001; Pratt et al., 2009; Rehbein et al., 2011; Zhang et al., 2012; Healy et al., 2014). We observed a particle type with the abundance of m/z 59 and to a lesser degree also m/z 74 (Fig. 2) that we interpret as organic particle containing amines. In addition, the fragmentation patterns of several single particle mass spectra show further peaks at m/z 86 ($(C_2H_5)_2NCH_2^+$) and m/z 101 (molecular peak of TMA) indicating detection of TMA (Angelino et al., 2001). Interestingly, the relative fraction of mass spectra containing signatures for amines is increased in the cloud residues (Fig. 6). Thus, the time series of the characteristic marker peak m/z 59 was compared to the concentrations of trimethylamine (TMA), dimethylamine (DMA) and methylamine (MA) measured in the cloud water samples by ion chromatography (Fig. 7). Caution is required because cobalt is an isobar to the amine fragment $(CH_3)_3N^+$ at m/z 59. But since cobalt was detected during HCCT-2010 only in very low concentration in the cloud water samples (Fomba et al., 2015), we ascribe the signal at m/z 59 to amine compounds. Due to the fact that cloud water sampling was not done continuously, the time series of AL-ABAMA and the amine species are only partly comparable. A reasonably good agreement is observed between the number of amine containing mass spectra per hour and the mass concentration of TMA (Pearson's $r = 0.60$) except for the disagreement around 17:00. Amine compounds in the atmosphere can originate from various sources (Ge et al., 2011). Besides from animal husbandry and biomass burning (Schade and Crutzen, 1995), TMA, DMA and MA can originate from, e.g., industrial processes (Ge et al., 2011) and have been observed in ambient air (Chang et al., 2003; Sellegri et al., 2005). An enhanced partitioning for gas phase trimethylamine (TMA) on pre-existing particles coated by an aqueous layer was observed at high relative humidity and low temperature (Rehbein et al., 2011; Zhang et al., 2012), thus the generally increased abundance of amines in cloud water may not be surprising. Whether amines remain in the aerosol phase after cloud droplet evaporation remains unclear, but may play an important role in cloud processing of aerosol particles.

3.2.3 Biomass burning and soot

The results also show an increased fraction of the particle type "soot" in cloud residues. Freshly emitted soot particles are hydrophobic and do not serve as CCN at realistic supersaturations (Dusek et al., 2006b; Koehler et al., 2009). Nevertheless, it was ob-
served in several studies that soot is more efficiently activated than organic particles (Hitzenberger et al., 2000; Sellegri et al., 2003). The size resolved aerosol composition (see Fig. 3) shows that the observed "soot" particles were mainly larger than 450 nm, leading to the conclusion that mostly aged soot particles were analysed by the mass spectrometer. Furthermore, the "soot" clusters reveal internal mixtures with soluble in-
organic compounds like nitrate or sulphate, which is presumably leading to activation of these particles at lower critical supersaturation (Dusek et al., 2006b; Henning et al., 2010). Internally mixed particles can either develop from condensation of secondary compounds on pre-existing particles or from coagulation with hygroscopic particles respectively cloud droplets. Due to the fact that even the out-of-cloud aerosol particles
that contain soot are internally mixed with secondary inorganic compounds, the increased fraction of soot particles in cloud residues can rather be explained by a good CCN activity of hygroscopic soot particles than caused by in-cloud impaction scavenging. Aging of atmospheric soot particles by coating with sulphate and nitrate has been observed using single particle mass spectrometry by Pratt and Prather (2010) as well
as by Moffet and Prather (2009). The authors concluded that such processing of soot particles in the urban environment of Mexico City takes about three hours. Although in a cleaner environment than Mexico City coating by nitrate and sulphate will likely be slower, it appears to be a reasonable explanation for the findings that soot-containing particles internally mixed with nitrate and sulphate are efficiently activated as CCN and
are therefore enhanced in cloud residues. The mass based scavenging efficiency was found to be markedly lower than that of sulphate or nitrate (Schneider et al., 2015), confirming the assumption that the large soot-containing particles (> 450 nm) found in the cloud residues contain soot only as a minor mass fraction.

The relative percentage of biomass burning particles occurring in the out-of-cloud aerosol does not differ much from that in the cloud residues. In agreement with previous observations (Ross et al., 2003; de Villiers et al., 2010) this implies that aerosol from biomass burning is an effective CCN, resulting from a high content of soluble organic and inorganic compounds in the particles (Silva et al., 1999; Posfai et al., 2003; Andreae and Rosenfeld, 2008; Pratt et al., 2011).

The high percentage of particles originating from combustion processes ("soot", "biomass burning", "diesel exhaust") of about 43 % (Fig. 6) is investigated more closely in the following. Figure 8 shows the time series of the particle types "soot" (blue, Fig. 8b) and the sum of all particle types containing elemental carbon (brown, Fig. 8c) observed by ALABAMA, along with temperature, concentration of equivalent black carbon (EBC) measured by the MAAP, and the biomass burning aerosol inferred from AMS data (green, Fig. 8d). The latter was estimated from the AMS data based on the marker peak at m/z 60 for Levoglucosan which is an indicator for biomass burning (Simoneit et al., 1999; Schneider et al., 2006; Alfarra et al., 2007). Conversion of f_{60} (fraction of m/z 60 in the total organic signal) into mass concentration was demonstrated by Weimer (2008) and Crippa et al. (2014). The time series of the "soot" particle type agrees only partly with the time series of EBC. A better agreement ($r = 0.47$) is reached if the time series of all clusters containing elemental carbon in the mean mass spectra ("soot", "diesel exhaust", "biomass burning") is compared to EBC. The three data sets (MAAP, ALABAMA, AMS) allow for the attribution of the events shown in Fig. 8 with enhanced EBC concentrations to different particle types: the event on 24 September 2010 (blue frame) is not caused by biomass burning but from combustion of other (most likely fossil) fuel (like coal, oil, diesel), because the biomass burning marker remains low. In contrast, the events from 10 October 2010 to 15 October 2010 and from 17 October 2010 to 19 October 2010 (green frame) can be mainly attributed to biomass burning. The short data gap on 17 October is due to technical issues. Furthermore the EBC concentration and the percentage of biomass burning particles rise with decreasing temperature (Fig. 8a). This can be attributed to the beginning of heating period and

consequently increased heating after 1 October 2010 leading to increased emission of from local and regional residential heating in the city Suhl and other smaller cities and villages in south-westerly direction (compare also Sect. 3.3).

3.2.4   Mineral dust and metals

Except for the particle type "Ca", the number fractions of mineral dust and metallic particle types ("Fe, V", "Ni" and "Pb") are markedly enhanced in the cloud residues. All these particles contain nitrate and sulphate, too (see Fig. 2), thus the good activation or scavenging efficiency is likely caused by the soluble compounds in these particles.

3.3   Cloud residue analysis for the full cloud events (FCE)

In the following the selected full cloud events (see Table 1) will be analysed in more detail. These cloud events represent a subset of all cloud measurements and are referring to certain conditions that were given in detail in Tilgner et al. (2014). The composition of the cloud residual particles measured during the individual FCE during HCCT-2010 are shown in Fig. 9. Also given are the number of analysed mass spectra and the averaged mass concentration of equivalent black carbon measured in the interstitial aerosol during the events. Only FCE with sufficient (> 100) number of mass spectra are considered. These individual events show large event-to-event variability, especially in the fraction of particles of the type "soot". Four FCE are characterized by a markedly higher fraction of "soot" particles, namely FCE 7.1, 11.2, 11.3 and 13.3, all of them between 24 September and 6 October. These events are also characterised by a high absolute mass concentration of EBC, especially FCE 11.2 and FCE 13.3 with about $300\,\mathrm{ng\,m^{-3}}$ of EBC. To further investigate this finding, the origin of the air masses encountered during these FCE is inspected by means of back trajectories. Figure 10 displays the 96 h-back trajectories, separated for the "low-soot FCE" (left) and the "high-soot FCE" (right). It becomes clear that the air masses encountered during the "low-soot FCE" arrive mainly from west/north west and have spent a considerable amount of the 96 h

prior to the measurement over the Atlantic Ocean (see also Fig. S1 in the Supplement to Tilgner et al., 2014). These air masses had less opportunity to accumulate pollution particles over the continent. In contrast, the "high-soot" air masses arrive more from south/south-west and have travelled slower, therefore having spent more time of the previous 96 h of land, leading to higher accumulation of anthropogenic emitted particles like soot. An exceptional case is FCE 22.0 (included in the left graph of Fig. 10), where the air masses arrive from east/north-east, although the local wind direction was south-west (as a prerequisite for an FCE). This air mass contained the highest fraction of biomass burning particles of all FCE and the highest number of mass spectra per event and time (1561 spectra in only 7.2 h, see Table 1). It has to be noted here that the full cloud events may not be representative for the general situation for clouds at the Schmücke, because of the selected data set. The composition data for the FCE are based on 4400 mass spectra, while for the composition of all cloud residues (Fig. 6) more than 13 000 mass spectra were analysed. For example, the required prerequisite that the local wind direction for an FCE has to be south-west, air masses of all FCE pass the city of Suhl located south-west of the Schmücke, which may lead to a higher relative amount of anthropogenic particles and a higher influence of local and regional emissions in the full cloud events compared to the general case. On the other hand, the analysis of the diurnal cycles in Sect. 3.1 has shown that in general local and regional sources have a high influence on the aerosol particle abundance.

3.4 Change of particle mixing state by cloud processing

As mentioned before, all identified particle types indicate internal mixtures with nitrate, sulphate or both species. Therefore the clustering algorithm can not provide information about the particle mixing state from out-of-cloud to inside of the cloud. Therefore, the mixing state of the particles with nitrate and sulphate was investigated by means of the characteristic marker peaks m/z -62 (NO_3^-) and m/z -97 (HSO_4^-).

To compare cloud residues and out-of-cloud aerosol, we selected air masses with comparable origins based on HYSPLIT back trajectories for in-cloud and out-of-cloud

conditions. As an additional criterion it was required that the local wind direction at the Schmücke was constant. The listed events "I" and "II" in Table 5 fulfilled these criteria. These events differ slightly from the defined FCEs because the criteria for the FCEs were not taken into account here. The cloud sampling phase of event "I" corresponds mostly to FCE1.1, while that of event "II" is a part of FCE24.0. During event "I" the air masses for in-cloud and out-of-cloud conditions both arrived from France, while air masses for both conditions during event "II" passed over England.

The characteristic marker peaks m/z -62 and m/z -97 in the single particle mass spectra of the events "I" and "II" show that only less than 1 % of the out-of-cloud aerosol particles contained neither nitrate nor sulphate for both events. Thus, 99 % of the out-of-cloud aerosol particles were already internally mixed with secondary inorganic compounds before passing the cloud. Such a high percentage of particles being internally mixed with secondary inorganic compounds were also found by single particle mass spectrometry during other studies in California (Cahill et al., 2012) or Harrow (Jeong et al., 2011). However, we observed an increase of the particle fraction containing nitrate in the cloud residues compared to the out-of-cloud aerosol, and the same finding holds for sulphate (Fig. 11, left). This can be explained by a more detailed analysis of the particle mixing state, distinguishing between particles containing only nitrate, only sulphate or both nitrate and sulphate (Fig. 11, right). Particles internally mixed only with sulphate (i.e. containing no nitrate) represent in general a minor fraction (< 3 %). For both analysed events the percentage of particles containing only nitrate and only sulphate was smaller in case of cloud residues compared to the out-of-cloud aerosol while the percentage of particles with nitrate and sulphate was increased. This observed increase indicates a sulphate addition to those particles that contained only nitrate, but also a nitrate addition to those particles that contained only sulphate. In the cloud residues, particles not containing nitrate can almost not be found. It must be noted that relative percentages of out-of-cloud aerosol particles internally mixed with secondary inorganics added for both events are less than the 99 % inferred above, due to the different threshold values that had to be used for the definition whether a peak

is present in a mass spectrum or not (see Supplement, chapter 3). This addition of sulphate and nitrate (and possibly also of organic components as amines, see 3.2.2) by cloud processing can also be observed in a size shift of the analysed particles. Figure 12 shows the size histograms of the particles analysed by ALABAMA during event I and II. In both cases a shift in the histogram to larger sizes is observed. The activation of CCN to cloud droplets is usually occurring at much smaller sizes (activation diameters upwind of the Schmücke have been observed to range between 123 and 194 nm, Henning et al., 2014), such that the observed size shift by ALABAMA can very likely be attributed to the uptake of gaseous species by the cloud droplets, leading to a size increase of the residual particles.

These two case studies demonstrate the change of the particle mixing state by chemical processes inside the cloud liquid phase. Similar observations were found earlier in numerous studies (e.g., Laj et al., 1997b; Sellegri et al., 2003; Brüggemann et al., 2005; McFiggans et al., 2006; Hayden et al., 2008; Zelenyuk et al., 2010). The enrichment of nitrate was also observed by simultaneous measurements with an AMS providing evidence of an increased mass concentration of nitrate in cloud residues compared to interstitial and out-of-cloud aerosol (Schneider et al., 2015). Such an enhancement of nitrate in cloud droplets can be explained by the uptake of gaseous nitric acid into the cloud droplets (Tilgner et al., 2005; Hayden et al., 2008). Enrichment of sulphate in cloud droplets can occur via different pathways. Besides the uptake of gaseous H_2SO_4 and the scavenging of ultrafine particulate matter also the uptake of SO_2 with subsequent oxidation plays a role (Harris et al., 2014). Furthermore Harris et al. (2013) could prove that besides the known SO_2 oxidation by H_2O_2 also the oxidation with O_2 catalysed by transition metals plays a significant role for the sulphate production. Despite the low number concentration of activated mineral dust particles in general, it became apparent that SO_2 oxidation was mainly catalysed by dissolved transition metals during HCCT-2010. As it was shown in this study, transition metals were also detected by the ALABAMA (see Table 2).

Furthermore the aerosol hygroscopicity was investigated in the same field experiment before and after cloud formation at the valley sites. In agreement with the described results, the hygroscopicity of the particles was found to be increased after passing the cloud (up to 50 %; see Henning et al., 2014). By means of the above described processes water-soluble material is enriched inside the particles while being processed by the cloud. After evaporation of the cloud the water-soluble material it is likely to remain in the particles, thereby increasing their hygroscopicity.

4   Summary and conclusions

During the HCCT-2010 campaign, more than 170 000 aerosol particles and more than 14 000 cloud residual particles were analysed by single particle mass spectrometry. The data evaluation was done by a combination of the clustering algorithm fuzzy *c*-means and the marker peak method, resulting in 14 different particle types. From the diurnal trends of the occurrence of these particle types, the influence of local and regional sources on the aerosol composition was estimated to be about 63 %. Especially the particle types "soot" and "biomass burning" could be allocated to local or regional sources. The single particle data further allowed for a better attribution of equivalent black carbon to different sources, as fossil fuel burning or biomass burning. Important local sources are the city Suhl in the predominant wind direction, together with the beginning of the heating period in October, leading to increased biomass burning signatures.

Analysis of the cloud residues revealed that the relative percentage of soot and amines is increased compared to out-of-cloud aerosol. Analysis of cloud water samples by ion chromatography showed that amines were mainly found in the form of trimethylamine. The increased fraction of soot can be explained by processing of soot particles leading to coating by nitrate and sulphate which is known to occur in a few hours. In addition the size resolved aerosol composition reveals that the detected particles

containing soot are larger than 450 nm. Both facts suggest that such processed soot particles are good cloud condensation nuclei.

All observed particle types show internal mixtures with the secondary inorganic compounds nitrate and/or sulphate. By means of the characteristic marker peaks m/z −62 and m/z −97 for nitrate respectively sulphate, the change of the particle mixing state from out-of-cloud to in-cloud was investigated in two case studies. In both cases the addition of nitrate and sulphate to the cloud droplets was observed. This finding is most likely due to the uptake of HNO_3 from the gas phase and sulphate production by the oxidation of SO_2 by transition metals and H_2O_2 inside the cloud droplets (Harris et al., 2014), besides the uptake of H_2SO_4.

Such a cloud processing of aerosol particles has important implications for the hygroscopic properties of the aerosol particles after cloud passage. An increase of soluble compounds in the particles, together with the involved growth of the particle size, will lead to an enhanced number of CCN that are available in the air mass after evaporation of the cloud. Additionally the modified chemical composition can lead to altered radiation properties concerning light scattering and absorption. Especially internal mixed soot particles indicate a higher absorption than pure soot particles (Jacobson, 2001) and could therefore counteract the cooling effect of clouds.

The Supplement related to this article is available online at doi:10.5194/acpd-15-24419-2015-supplement.

References

Alfarra, M. R., Prevot, A. S. H., Szidat, S., Sandradewi, J., Weimer, S., Lanz, V. A., Schreiber, D., Mohr, M., and Baltensperger, U.: Identification of the mass spectral signature of organic aerosols from wood burning emissions, Environ. Sci. Technol., 41, 5770–5777, doi:10.1021/es062289b, 2007.

Allan, J. D., Baumgardner, D., Raga, G. B., Mayol-Bracero, O. L., Morales-García, F., García-García, F., Montero-Martínez, G., Borrmann, S., Schneider, J., Mertes, S., Walter, S., Gysel, M., Dusek, U., Frank, G. P., and Krämer, M.: Clouds and aerosols in Puerto Rico – a new evaluation, Atmos. Chem. Phys., 8, 1293–1309, doi:10.5194/acp-8-1293-2008, 2008.

Andreae, M. O. and Rosenfeld, D.: Aerosol-cloud-precipitation interactions. Part 1. The nature and sources of cloud-active aerosols, Earth-Sci. Rev., 89, 13–41, doi:10.1016/j.earscirev.2008.03.001, 2008.

Angelino, S., Suess, D. T., and Prather, K. A.: Formation of aerosol particles from reactions of secondary and tertiary alkylamines: characterization by aerosol time-of-flight mass spectrometry, Environ. Sci. Technol., 35, 3130–3138, doi:10.1021/es0015444, 2001.

Ault, A. P., Moore, M. J., Furutani, H., and Prather, K. A.: Impact of emissions from the Los Angeles port region on San Diego air quality during regional transport events, Environ. Sci. Technol., 43, 3500–3506, doi:10.1021/es8018918, 2009.

Ault, A. P., Gaston, C. J., Wang, Y., Dominguez, G., Thiemens, M. H., and Prather, K. A.: Characterization of the single particle mixing state of individual ship plume events measured at the port of Los Angeles, Environ. Sci. Technol., 44, 1954–1961, doi:10.1021/es902985h, 2010.

Bein, K. J., Zhao, Y. J., Wexler, A. S., and Johnston, M. V.: Speciation of size-resolved individual ultrafine particles in Pittsburgh, Pennsylvania, J. Geophys. Res.-Atmos., 110, D07S05, doi:10.1029/2004jd004708, 2005.

Bezdek, J. C.: Pattern Recognition with Fuzzy Objective Function Algorithms, Plenum Press, New York, USA, 1981.

Bezdek, J. C., Ehrlich, R., and Full, W.: FCM – the fuzzy c-means clustering-algorithm, Comput. Geosci., 10, 191–203, doi:10.1016/0098-3004(84)90020-7, 1984.

Bower, K. N., Hill, T. A., Coe, H., and Choularton, T. W.: SO2 oxidation in an entraining cloud model with explicit microphysics, Atmos. Environ. A-Gen., 25, 2401–2418, doi:10.1016/0960-1686(91)90114-m, 1991.

Bower, K. N., Choularton, T. W., Gallagher, M. W., Colvile, R. N., Wells, M., Beswick, K. M., Wiedensohler, A., Hansson, H. C., Svenningsson, B., Swietlicki, E., Wendisch, M., Berner, A., Kruisz, C., Laj, P., Facchini, M. C., Fuzzi, S., Bizjak, M., Dollard, G., Jones, B., Acker, K., Wieprecht, W., Preiss, M., Sutton, M. A., Hargreaves, K. J., StoretonWest, R. L., Cape, J. N., and Arends, B. G.: Observations and modelling of the processing of aerosol by a hill cap cloud, Atmos. Environ., 31, 2527–2543, doi:10.1016/s1352-2310(96)00317-2, 1997.

Brands, M., Kamphus, M., Böttger, T., Schneider, J., Drewnick, F., Roth, A., Curtius, J., Voigt, C., Borbon, A., Beekmann, M., Bourdon, A., Perrin, T., and Borrmann, S.: Characterization of a newly developed Aircraft-Based Laser Ablation Aerosol Mass spectrometer (ALABAMA) and first field deployment in urban pollution plumes over Paris during MEGAPOLI 2009, Aerosol Sci. Tech., 45, 46–64, doi:10.1080/02786826.2010.517813, 2011.

Brüggemann, E., Gnauk, T., Mertes, S., Acker, K., Auel, R., Wieprecht, W., Möller, D., Collett, J. L., Chang, H., Galgon, D., Chemnitzer, R., Rud, C., Junek, R., Wiedensohler, W., and Herrmann, H.: Schmücke hill cap cloud and valley stations aerosol characterisation during FEBUKO (I): particle size distribution, mass, and main components, Atmos. Environ., 39, 4291–4303, doi:10.1016/j.atmosenv.2005.02.013, 2005.

Cahill, J. F., Suski, K., Seinfeld, J. H., Zaveri, R. A., and Prather, K. A.: The mixing state of carbonaceous aerosol particles in northern and southern California measured during CARES and CalNex 2010, Atmos. Chem. Phys., 12, 10989–11002, doi:10.5194/acp-12-10989-2012, 2012.

Chang, I. H., Lee, C. G., and Lee, D. S.: Development of an automated method for simultaneous determination of low molecular weight aliphatic amines and ammonia in ambient air by diffusion scrubber coupled to ion chromatography, Anal. Chem., 75, 6141–6146, doi:10.1021/ac0347314, 2003.

Corbin, J. C., Rehbein, P. J. G., Evans, G. J., and Abbatt, J. P. D.: Combustion particles as ice nuclei in an urban environment: evidence from single-particle mass spectrometry, Atmos. Environ., 51, 286–292, doi:10.1016/j.atmosenv.2012.01.007, 2012.

Title Page

Abstract | Introduction

Conclusions | References

Tables | Figures

◀ | ▶

◀ | ▶

Back | Close

Full Screen / Esc

Printer-friendly Version

Interactive Discussion

Crippa, M., DeCarlo, P. F., Slowik, J. G., Mohr, C., Heringa, M. F., Chirico, R., Poulain, L., Freutel, F., Sciare, J., Cozic, J., Di Marco, C. F., Elsasser, M., Nicolas, J. B., Marchand, N., Abidi, E., Wiedensohler, A., Drewnick, F., Schneider, J., Borrmann, S., Nemitz, E., Zimmermann, R., Jaffrezo, J.-L., Prévôt, A. S. H., and Baltensperger, U.: Wintertime aerosol chemical composition and source apportionment of the organic fraction in the metropolitan area of Paris, Atmos. Chem. Phys., 13, 961–981, doi:10.5194/acp-13-961-2013, 2013.

Crippa, M., Canonaco, F., Lanz, V. A., Äijälä, M., Allan, J. D., Carbone, S., Capes, G., Ceburnis, D., Dall'Osto, M., Day, D. A., DeCarlo, P. F., Ehn, M., Eriksson, A., Freney, E., Hildebrandt Ruiz, L., Hillamo, R., Jimenez, J. L., Junninen, H., Kiendler-Scharr, A., Kortelainen, A.-M., Kulmala, M., Laaksonen, A., Mensah, A. A., Mohr, C., Nemitz, E., O'Dowd, C., Ovadnevaite, J., Pandis, S. N., Petäjä, T., Poulain, L., Saarikoski, S., Sellegri, K., Swietlicki, E., Tiitta, P., Worsnop, D. R., Baltensperger, U., and Prévôt, A. S. H.: Organic aerosol components derived from 25 AMS data sets across Europe using a consistent ME-2 based source apportionment approach, Atmos. Chem. Phys., 14, 6159–6176, doi:10.5194/acp-14-6159-2014, 2014.

Dall'Osto, M. and Harrison, R. M.: Chemical characterisation of single airborne particles in Athens (Greece) by ATOFMS, Atmos. Environ., 40, 7614–7631, doi:10.1016/j.atmosenv.2006.06.053, 2006.

Dall'Osto, M., Beddows, D. C. S., Kinnersley, R. P., Harrison, R. M., Donovan, R. J., and Heal, M. R.: Characterization of individual airborne particles by using aerosol time-of-flight mass spectrometry at Mace Head, Ireland, J. Geophys. Res.-Atmos., 109, D21302, doi:10.1029/2004jd004747, 2004.

Dall'Osto, M., Harrison, R. M., Coe, H., Williams, P. I., and Allan, J. D.: Real time chemical characterization of local and regional nitrate aerosols, Atmos. Chem. Phys., 9, 3709–3720, doi:10.5194/acp-9-3709-2009, 2009.

Dall'Osto, M., Harrison, R. M., Highwood, E. J., O'Dowd, C., Ceburnis, D., Querol, X., and Achterberg, E. P.: Variation of the mixing state of Saharan dust particles with atmospheric transport, Atmos. Environ., 44, 3135–3146, doi:10.1016/j.atmosenv.2010.05.030, 2010.

DeCarlo, P. F., Kimmel, J. R., Trimborn, A., Northway, M. J., Jayne, J. T., Aiken, A. C., Gonin, M., Fuhrer, K., Horvath, T., Docherty, K. S., Worsnop, D. R., and Jimenez, J. L.: Field-deployable, high-resolution, time-of-flight aerosol mass spectrometer, Anal. Chem., 78, 8281–8289, doi:10.1021/ac061249n, 2006.

Title Page

Abstract | Introduction

Conclusions | References

Tables | Figures

|◄ | ►|

◄ | ►

Back | Close

Full Screen / Esc

Printer-friendly Version

Interactive Discussion

de Villiers, R. A., Ancellet, G., Pelon, J., Quennehen, B., Schwarzenboeck, A., Gayet, J. F., and Law, K. S.: Airborne measurements of aerosol optical properties related to early spring transport of mid-latitude sources into the Arctic, Atmos. Chem. Phys., 10, 5011–5030, doi:10.5194/acp-10-5011-2010, 2010.

Draxler, R. R. and Rolph, G. D.: HYSPLIT (HYbrid Single-Particle Lagrangian Integrated Trajectory) Model access via NOAA ARL READY Website, available at: http://ready.arl.noaa.gov/HYSPLIT.php (last access: 18 August 2015), NOAA Air Resources Laboratory, Silver Spring, MD, 2012.

Drewnick, F., Hings, S. S., DeCarlo, P., Jayne, J. T., Gonin, M., Fuhrer, K., Weimer, S., Jimenez, J. L., Demerjian, K. L., Borrmann, S., and Worsnop, D. R.: A new time-of-flight aerosol mass spectrometer (TOF-AMS) – instrument description and first field deployment, Aerosol Sci. Tech., 39, 637–658, doi:10.1080/02786820500182040, 2005.

Drewnick, F., Schneider, J., Hings, S. S., Hock, N., Noone, K., Targino, A., Weimer, S., and Borrmann, S.: Measurement of ambient, interstitial, and residual aerosol particles on a mountaintop site in central Sweden using an aerosol mass spectrometer and a CVI, J. Atmos. Chem., 56, 1–20, 2007.

Dusek, U., Frank, G. P., Hildebrandt, L., Curtius, J., Schneider, J., Walter, S., Chand, D., Drewnick, F., Hings, S., Jung, D., Borrmann, S., and Andreae, M. O.: Size matters more than chemistry for cloud-nucleating ability of aerosol particles, Science, 312, 1375–1378, 2006a.

Dusek, U., Reischl, G. P., and Hitzenberger, R.: CCN activation of pure and coated carbon black particles, Environ. Sci. Technol., 40, 1223–1230, doi:10.1021/es0503478, 2006b.

Facchini, M. C., Decesari, S., Rinaldi, M., Carbone, C., Finessi, E., Mircea, M., Fuzzi, S., Moretti, F., Tagliavini, E., Ceburnis, D., and O'Dowd, C. D.: Important source of marine secondary organic aerosol from biogenic amines, Environ. Sci. Technol., 42, 9116–9121, doi:10.1021/es8018385, 2008.

Fomba, K. W., van Pinxteren, D., Müller, K., Iinuma, Y., Lee, T., Collett Jr., J. L., and Herrmann, H.: Trace metal characterization of aerosol particles and cloud water during HCCT 2010, Atmos. Chem. Phys., 15, 8751–8765, doi:10.5194/acp-15-8751-2015, 2015.

Fuzzi, S., Facchini, M. C., Schell, D., Wobrock, W., Winkler, P., Arends, B. G., Kessel, M., Möls, J. J., Pahl, S., Schneider, T., Berner, A., Solly, I., Kruisz, C., Kalina, M., Fierlinger, H., Hallberg, A., Vitali, P., Santoli, L., and Tigli, G.: Multiphase chemistry and acidity of clouds at Kleiner Feldberg, J. Atmos. Chem., 19, 87–106, doi:10.1007/BF00696584, 1994.

Title Page

Abstract	Introduction
Conclusions	References
Tables	Figures

◀◀ ▶▶

◀ ▶

Back Close

Full Screen / Esc

Printer-friendly Version

Interactive Discussion

Ge, X., Wexler, A. S., and Clegg, S. L.: Atmospheric amines – Part I. A review, Atmos. Environ., 45, 524–546, doi:10.1016/j.atmosenv.2010.10.012, 2011.

Gieray, R., Wieser, P., Engelhardt, T., Swietlicki, E., Hansson, H. C., Mentes, B., Orsini, D., Martinsson, B., Svenningsson, B., Noone, K. J., and Heintzenberg, J.: Phase partitioning of aerosol constituents in cloud based on single-particle and bulk analysis, Atmos. Environ., 31, 2491–2502, doi:10.1016/s1352-2310(96)00298-1, 1997.

Gunthe, S. S., King, S. M., Rose, D., Chen, Q., Roldin, P., Farmer, D. K., Jimenez, J. L., Artaxo, P., Andreae, M. O., Martin, S. T., and Pöschl, U.: Cloud condensation nuclei in pristine tropical rainforest air of Amazonia: size-resolved measurements and modeling of atmospheric aerosol composition and CCN activity, Atmos. Chem. Phys., 9, 7551–7575, doi:10.5194/acp-9-7551-2009, 2009.

Hallberg, A., Ogren, J. A., Noone, K. J., Okada, K., Heintzenberg, J., and Svenningsson, I. B.: The influence of aerosol particle composition on cloud droplet formation, J. Atmos. Chem., 19, 153–171, doi:10.1007/BF00696587, 1994.

Harris, E., Sinha, B., van Pinxteren, D., Tilgner, A., Fomba, K. W., Schneider, J., Roth, A., Gnauk, T., Fahlbusch, B., Mertes, S., Lee, T., Collett, J., Foley, S., Borrmann, S., Hoppe, P., and Herrmann, H.: Enhanced role of transition metal ion catalysis during in-cloud oxidation of SO_2, Science, 340, 727–730, doi:10.1126/science.1230911, 2013.

Harris, E., Sinha, B., van Pinxteren, D., Schneider, J., Poulain, L., Collett, J., D'Anna, B., Fahlbusch, B., Foley, S., Fomba, K. W., George, C., Gnauk, T., Henning, S., Lee, T., Mertes, S., Roth, A., Stratmann, F., Borrmann, S., Hoppe, P., and Herrmann, H.: In-cloud sulfate addition to single particles resolved with sulfur isotope analysis during HCCT-2010, Atmos. Chem. Phys., 14, 4219–4235, doi:10.5194/acp-14-4219-2014, 2014.

Hayden, K. L., Macdonald, A. M., Gong, W., Toom-Sauntry, D., Anlauf, K. G., Leithead, A., Li, S. M., Leaitch, W. R., and Noone, K.: Cloud processing of nitrate, J. Geophys. Res.-Atmos., 113, D18201 doi:10.1029/2007jd009732, 2008.

Healy, R., Evans, G., Murphy, M., Sierau, B., Arndt, J., McGillicuddy, E., O'Connor, I., Sodeau, J., and Wenger, J.: Single-particle speciation of alkylamines in ambient aerosol at five European sites, Anal. Bioanal. Chem., 407, 1–11, doi:10.1007/s00216-014-8092-1, 2014.

Henning, S., Wex, H., Hennig, T., Kiselev, A., Snider, J. R., Rose, D., Dusek, U., Frank, G. P., Poschl, U., Kristensson, A., Bilde, M., Tillmann, R., Kiendler-Scharr, A., Mentel, T. F., Walter, S., Schneider, J., Wennrich, C., and Stratmann, F.: Soluble mass, hygroscopic growth,

and droplet activation of coated soot particles during LACIS Experiment in November (LExNo), J. Geophys. Res.-Atmos., 115, D11206, doi:10.1029/2009jd012626, 2010.

Henning, S., Dieckmann, K., Ignatius, K., Schäfer, M., Zedler, P., Harris, E., Sinha, B., van Pinxteren, D., Mertes, S., Birmili, W., Merkel, M., Wu, Z., Wiedensohler, A., Wex, H., Herrmann, H., and Stratmann, F.: Influence of cloud processing on CCN activation behaviour in the Thuringian Forest, Germany during HCCT-2010, Atmos. Chem. Phys., 14, 7859–7868, doi:10.5194/acp-14-7859-2014, 2014.

Herrmann, H., Wolke, R., Müller, K., Brüggemann, E., Gnauk, T., Barzaghi, P., Mertes, S., Lehmann, K., Massling, A., Birmili, W., Wiedensohler, A., Wieprecht, W., Acker, K., Jaeschke, W., Kramberger, H., Svrcina, B., Bachmann, K., Collett, J. L., Galgon, D., Schwirn, K., Nowak, A., van Pinxteren, D., Plewka, A., Chemnitzer, R., Rud, C., Hofmann, D., Tilgner, A., Diehl, K., Heinold, B., Hinneburg, D., Knoth, O., Sehili, A. M., Simmel, M., Wurzler, S., Majdik, Z., Mauersberger, G., and Müller, F.: FEBUKO and MODMEP: field measurements and modelling of aerosol and cloud multiphase processes, Atmos. Environ., 39, 4169–4183, doi:10.1016/j.atmosenv.2005.02.004, 2005.

Hinz, K. P. and Spengler, B.: Instrumentation, data evaluation and quantification in on-line aerosol mass spectrometry, J. Mass Spectrom., 42, 843–860, 2007.

Hinz, K. P., Greweling, M., Drews, F., and Spengler, B.: Data processing in on-line laser mass spectrometry of inorganic, organic, or biological airborne particles, J. Am. Soc. Mass Spectr., 10, 648–660, doi:10.1016/s1044-0305(99)00028-8, 1999.

Hinz, K. P., Erdmann, N., Gruning, C., and Spengler, B.: Comparative parallel characterization of particle populations with two mass spectrometric systems LAMPAS 2 and SPASS, Int. J. Mass Spectrom., 258, 151–166, doi:10.1016/j.ijms.2006.09.008, 2006.

Hitzenberger, R., Berner, A., Kromp, R., Kasper-Giebl, A., Limbeck, A., Tscherwenka, W., and Puxbaum, H.: Black carbon and other species at a high-elevation European site (Mount Sonnblick, 3106 m, Austria): concentrations and scavenging efficiencies, J. Geophys. Res.-Atmos., 105, 24637–24645, doi:10.1029/2000jd900349, 2000.

Jacobson, M. Z.: Strong radiative heating due to the mixing state of black carbon in atmospheric aerosols, Nature, 409, 695–697, doi:10.1038/35055518, 2001.

Jeong, C.-H., McGuire, M. L., Godri, K. J., Slowik, J. G., Rehbein, P. J. G., and Evans, G. J.: Quantification of aerosol chemical composition using continuous single particle measurements, Atmos. Chem. Phys., 11, 7027–7044, doi:10.5194/acp-11-7027-2011, 2011.

Kamphus, M., Ettner-Mahl, M., Klimach, T., Drewnick, F., Keller, L., Cziczo, D. J., Mertes, S., Borrmann, S., and Curtius, J.: Chemical composition of ambient aerosol, ice residues and cloud droplet residues in mixed-phase clouds: single particle analysis during the Cloud and Aerosol Characterization Experiment (CLACE 6), Atmos. Chem. Phys., 10, 8077–8095, doi:10.5194/acp-10-8077-2010, 2010.

Klimach, T.: Chemische Zusammensetzung der Aerosole: Design und Datenauswertung eines Einzelpartikel-Laserablationsmassenspektrometers, Johannes Gutenberg-Universität, Mainz, Germany, 2012.

Koehler, K. A., DeMott, P. J., Kreidenweis, S. M., Popovicheva, O. B., Petters, M. D., Carrico, C. M., Kireeva, E. D., Khokhlova, T. D., and Shonija, N. K.: Cloud condensation nuclei and ice nucleation activity of hydrophobic and hydrophilic soot particles, Phys. Chem. Chem. Phys., 11, 7906–7920, doi:10.1039/B905334b, 2009.

Korn, M. D. A., dos Santos, D. S. S., Welz, B., Vale, M. G. R., Teixeira, A. P., Lima, D. D., and Ferreira, S. L. C.: Atomic spectrometric methods for the determination of metals and metalloids in automotive fuels – a review, Talanta, 73, 1–11, doi:10.1016/j.talanta.2007.03.036, 2007.

Laj, P., Fuzzi, S., Facchini, M. C., Lind, J. A., Orsi, G., Preiss, M., Maser, R., Jaeschke, W., Seyffer, E., Helas, G., Acker, K., Wieprecht, W., Moller, D., Arends, B. G., Mols, J. J., Colvile, R. N., Gallagher, M. W., Beswick, K. M., Hargreaves, K. J., StoretonWest, R. L., and Sutton, M. A.: Cloud processing of soluble gases, Atmos. Environ., 31, 2589–2598, doi:10.1016/s1352-2310(97)00040-x, 1997a.

Laj, P., Fuzzi, S., Facchini, M. C., Orsi, G., Berner, A., Kruisz, C., Wobrock, W., Hallberg, A., Bower, K. N., Gallagher, M. W., Beswick, K. M., Colvile, R. N., Choularton, T. W., Nason, P., and Jones, B.: Experimental evidence for in-cloud production of aerosol sulphate, Atmos. Environ., 31, 2503–2514, doi:10.1016/s1352-2310(96)00217-8, 1997b.

Lanz, V. A., Prévôt, A. S. H., Alfarra, M. R., Weimer, S., Mohr, C., DeCarlo, P. F., Gianini, M. F. D., Hueglin, C., Schneider, J., Favez, O., D'Anna, B., George, C., and Baltensperger, U.: Characterization of aerosol chemical composition with aerosol mass spectrometry in Central Europe: an overview, Atmos. Chem. Phys., 10, 10453–10471, doi:10.5194/acp-10-10453-2010, 2010.

Limbeck, A. and Puxbaum, H.: Dependence of in-cloud scavenging of polar organic aerosol compounds on the water solubility, J. Geophys. Res.-Atmos., 105, 19857–19867, doi:10.1029/2000jd900123, 2000.

Liu, P., Ziemann, P. J., Kittelson, D. B., and McMurry, P. H.: Generating particle beams of controlled dimensions and divergence: 2. Experimental evaluation of particle motion in aerodynamic lenses and nozzle expansions, Aerosol Sci. Tech., 22, 314–324, 1995a.

Liu, P., Ziemann, P. J., Kittelson, D. B., and McMurry, P. H.: Generating particle beams of controlled dimensions and divergence: 1. Theory of particle motion in aerodynamic lenses and nozzle expansions, Aerosol Sci. Tech., 22, 293–313, 1995b.

McFiggans, G., Artaxo, P., Baltensperger, U., Coe, H., Facchini, M. C., Feingold, G., Fuzzi, S., Gysel, M., Laaksonen, A., Lohmann, U., Mentel, T. F., Murphy, D. M., O'Dowd, C. D., Snider, J. R., and Weingartner, E.: The effect of physical and chemical aerosol properties on warm cloud droplet activation, Atmos. Chem. Phys., 6, 2593–2649, doi:10.5194/acp-6-2593-2006, 2006.

Mertes, S., Galgon, D., Schwirn, K., Nowak, A., Lehmann, K., Massling, A., Wiedensohler, A., and Wieprecht, W.: Evolution of particle concentration and size distribution observed upwind, inside and downwind hill cap clouds at connected flow conditions during FEBUKO, Atmos. Environ., 39, 4233–4245, doi:10.1016/j.atmosenv.2005.02.009, 2005a.

Mertes, S., Lehmann, K., Nowak, A., Massling, A., and Wiedensohler, A.: Link between aerosol hygroscopic growth and droplet activation observed for hill-capped clouds at connected flow conditions during FEBUKO, Atmos. Environ., 39, 4247–4256, doi:10.1016/j.atmosenv.2005.02.010, 2005b.

Middlebrook, A. M., Murphy, D. M., Lee, S.-H., Thomson, D. S., Prather, K. A., Wenzel, R. J., Liu, D.-Y., Phares, D. J., Rhoads, K. P., Wexler, A. S., Johnston, M. V., Jimenez, J. L., Jayne, J. T., Worsnop, D. R., Yourshaw, I., Seinfeld, J. H., and Flagan, R. C.: A comparison of particle mass spectrometers during the 1999 Atlanta Supersite Project, J. Geophys. Res., 108, 8424, doi:10.1029/2001JD000660, 2003.

Moffet, R. C. and Prather, K. A.: In-situ measurements of the mixing state and optical properties of soot with implications for radiative forcing estimates, P. Natl. Acad. Sci. USA, 106, 11872–11877, doi:10.1073/pnas.0900040106, 2009.

Murphy, D. M., Middlebrook, A. M., and Warshawsky, M.: Cluster analysis of data from the Particle Analysis by Laser Mass Spectrometry (PALMS) instrument, Aerosol Sci. Tech., 37, 382–391, doi:10.1080/02786820300971, 2003.

Ogren, J. A., Heintzenberg, J., and Charlson, R. J.: Insitu sampling of clouds with a droplet to aerosol converter, Geophys. Res. Lett., 12, 121–124, doi:10.1029/GL012i003p00121, 1985.

Title Page

Abstract | Introduction

Conclusions | References

Tables | Figures

|◄ | ►|

◄ | ►

Back | Close

Full Screen / Esc

Printer-friendly Version

Interactive Discussion

Petzold, A., Ogren, J. A., Fiebig, M., Laj, P., Li, S.-M., Baltensperger, U., Holzer-Popp, T., Kinne, S., Pappalardo, G., Sugimoto, N., Wehrli, C., Wiedensohler, A., and Zhang, X.-Y.: Recommendations for reporting "black carbon" measurements, Atmos. Chem. Phys., 13, 8365–8379, doi:10.5194/acp-13-8365-2013, 2013.

Posfai, M., Simonics, R., Li, J., Hobbs, P. V., and Buseck, P. R.: Individual aerosol particles from biomass burning in southern Africa: 1. Compositions and size distributions of carbonaceous particles, J. Geophys. Res.-Atmos., 108, 8483, doi:10.1029/2002jd002291, 2003.

Pratt, K. A. and Prather, K. A.: Aircraft measurements of vertical profiles of aerosol mixing states, J. Geophys. Res.-Atmos., 115, D11305, doi:10.1029/2009jd013150, 2010.

Pratt, K. A., Hatch, L. E., and Prather, K. A.: Seasonal volatility dependence of ambient particle phase amines, Environ. Sci. Technol., 43, 5276–5281, doi:10.1021/es803189n, 2009.

Pratt, K. A., Twohy, C. H., Murphy, S. M., Moffet, R. C., Heymsfield, A. J., Gaston, C. J., DeMott, P. J., Field, P. R., Henn, T. R., Rogers, D. C., Gilles, M. K., Seinfeld, J. H., and Prather, K. A.: Observation of playa salts as nuclei in orographic wave clouds, J. Geophys. Res.-Atmos., 115, D15301, doi:10.1029/2009jd013606, 2010.

Pratt, K. A., Murphy, S. M., Subramanian, R., DeMott, P. J., Kok, G. L., Campos, T., Rogers, D. C., Prenni, A. J., Heymsfield, A. J., Seinfeld, J. H., and Prather, K. A.: Flight-based chemical characterization of biomass burning aerosols within two prescribed burn smoke plumes, Atmos. Chem. Phys., 11, 12549–12565, doi:10.5194/acp-11-12549-2011, 2011.

Rehbein, P. J. G., Jeong, C. H., McGuire, M. L., Yao, X. H., Corbin, J. C., and Evans, G. J.: Cloud and fog processing enhanced gas-to-particle partitioning of trimethylamine, Environ. Sci. Technol., 45, 4346–4352, doi:10.1021/es1042113, 2011.

Ross, K. E., Piketh, S. J., Bruintjes, R. T., Burger, R. P., Swap, R. J., and Annegarn, H. J.: Spatial and seasonal variations in CCN distribution and the aerosol-CCN relationship over southern Africa, J. Geophys. Res.-Atmos., 108, 8481, doi:10.1029/2002jd002384, 2003.

Schade, G. W. and Crutzen, P. J.: Emission of alphatic-amines from animal husbandry and their reactions – potential source of N_2O and HCN, J. Atmos. Chem., 22, 319–346, doi:10.1007/bf00696641, 1995.

Schneider, J., Weimer, S., Drewnick, F., Borrmann, S., Helas, G., Gwaze, P., Schmid, O., Andreae, M. O., and Kirchner, U.: Mass spectrometric analysis and aerodynamic properties of various types of combustion-related aerosol particles, Int. J. Mass Spectrom., 258, 37–49, 2006.

Title Page

Abstract | Introduction

Conclusions | References

Tables | Figures

|◄ | ►|

◄ | ►

Back | Close

Full Screen / Esc

Printer-friendly Version

Interactive Discussion

Schneider, J., Mertes, S., van Pinxteren, D., Herrmann, H., and Borrmann, S.: In-situ mass spectrometric analysis of cloud residuals and interstitial aerosol composition on orographic clouds during HCCT-2010: Uptake of nitric acid in cloud droplets, Atmos. Chem. Phys., in preparation, 2015.

Sedlak, D. L., Hoigne, J., David, M. M., Colvile, R. N., Seyffer, E., Acker, K., Wiepercht, W., Lind, J. A., and Fuzzi, S.: The cloudwater chemistry of iron and copper at Great Dun Fell, UK, Atmos. Environ., 31, 2515–2526, doi:10.1016/s1352-2310(96)00080-5, 1997.

Sellegri, K., Laj, P., Dupuy, R., Legrand, M., Preunkert, S., and Putaud, J. P.: Size-dependent scavenging efficiencies of multicomponent atmospheric aerosols in clouds, J. Geophys. Res.-Atmos., 108, 4334, doi:10.1029/2002jd002749, 2003.

Sellegri, K., Umann, B., Hanke, M., and Arnold, F.: Deployment of a ground-based CIMS apparatus for the detection of organic gases in the boreal forest during the QUEST campaign, Atmos. Chem. Phys., 5, 357–372, doi:10.5194/acp-5-357-2005, 2005.

Shields, L. G., Suess, D. T., and Prather, K. A.: Determination of single particle mass spectral signatures from heavy-duty diesel vehicle emissions for $PM_{2.5}$ source apportionment, Atmos. Environ., 41, 3841–3852, doi:10.1016/j.atmosenv.2007.01.025, 2007.

Silva, P. J. and Prather, K. A.: Interpretation of mass spectra from organic compounds in aerosol time-of-flight mass spectrometry, Anal. Chem., 72, 3553–3562, 2000.

Silva, P. J., Liu, D. Y., Noble, C. A., and Prather, K. A.: Size and chemical characterization of individual particles resulting from biomass burning of local Southern California species, Environ. Sci. Technol., 33, 3068–3076, doi:10.1021/es980544p, 1999.

Silva, P. J., Carlin, R. A., and Prather, K. A.: Single particle analysis of suspended soil dust from Southern California, Atmos. Environ., 34, 1811–1820, doi:10.1016/s1352-2310(99)00338-6, 2000.

Simoneit, B. R. T., Schauer, J. J., Nolte, C. G., Oros, D. R., Elias, V. O., Fraser, M. P., Rogge, W. F., and Cass, G. R.: Levoglucosan, a tracer for cellulose in biomass burning and atmospheric particles, Atmos. Environ., 33, 173–182, 1999.

Snyder, D. C., Schauer, J. J., Gross, D. S., and Turner, J. R.: Estimating the contribution of point sources to atmospheric metals using single-particle mass spectrometry, Atmos. Environ., 43, 4033–4042, doi:10.1016/j.atmosenv.2009.05.011, 2009.

Sodeman, D. A., Toner, S. M., and Prather, K. A.: Determination of single particle mass spectral signatures from light-duty vehicle emissions, Environ. Sci. Technol., 39, 4569–4580, doi:10.1021/es0489947, 2005.

Title Page

Abstract | Introduction

Conclusions | References

Tables | Figures

|◄ | ►|

◄ | ►

Back | Close

Full Screen / Esc

Printer-friendly Version

Interactive Discussion

Tilgner, A., Majdik, Z., Sehili, A. M., Simmel, M., Wolke, R., and Herrmann, H.: SPACCIM: simulations of the multiphase chemistry occurring in the FEBUKO hill cap cloud experiments, Atmos. Environ., 39, 4389–4401, doi:10.1016/j.atmosenv.2005.02.028, 2005.

Tilgner, A., Schöne, L., Bräuer, P., van Pinxteren, D., Hoffmann, E., Spindler, G., Styler, S. A., Mertes, S., Birmili, W., Otto, R., Merkel, M., Weinhold, K., Wiedensohler, A., Deneke, H., Schrödner, R., Wolke, R., Schneider, J., Haunold, W., Engel, A., Wéber, A., and Herrmann, H.: Comprehensive assessment of meteorological conditions and airflow connectivity during HCCT-2010, Atmos. Chem. Phys., 14, 9105–9128, doi:10.5194/acp-14-9105-2014, 2014.

Tolocka, M. P., Lake, D. A., Johnston, M. V., and Wexler, A. S.: Number concentrations of fine and ultrafine particles containing metals, Atmos. Environ., 38, 3263–3273, doi:10.1016/j.atmosenv.2004.03.010, 2004.

Trimborn, A., Hinz, K. P., and Spengler, B.: Online analysis of atmospheric particles with a transportable laser mass spectrometer during LACE 98, J. Geophys. Res., 107, LAC 13-11–LAC 13-10, 2002.

van Pinxteren, M., Fiedler, B., van Pinxteren, D., Iinuma, Y., Körtzinger, A., and Herrmann, H.: Chemical characterization of sub-micrometer aerosol particles in the tropical Atlantic Ocean: marine and biomass burning influences, J. Atmos. Chem., 72, 105–125, doi:10.1007/s10874-015-9307-3, 2015.

Vogt, R., Kirchner, U., Scheer, V., Hinz, K. P., Trimborn, A., and Spengler, B.: Identification of diesel exhaust particles at an Autobahn, urban and rural location using single-particle mass spectrometry, J. Aerosol. Sci., 34, 319–337, doi:10.1016/s0021-8502(02)00179-9, 2003.

Weimer, S.: Particle emission traffic and wood combustion and its impact on spatial distributions of submicron particulate matter, PhD thesis, Eidgenössische Technische Hochschule Zürich, Zürich, Switzerland, 2008.

Wendisch, M. and Brenguier, J.-L.: Airborne Measurements for Environmental Research: Methods and Instruments, Wiley-VCH Verlag GmbH and Co. KGaA, Weinheim, Germany, 2013.

Wobrock, W., Schell, D., Maser, R., Jaeschke, W., Georgii, H. W., Wieprecht, W., Arends, B. G., Mols, J. J., Kos, G. P. A., Fuzzi, S., Facchini, M. C., Orsi, G., Berner, A., Solly, I., Kruisz, C., Svenningsson, I. B., Wiedensohler, A., Hansson, H. C., Ogren, J. A., Noone, K. J., Hallberg, A., Pahl, S., Schneider, T., Winkler, P., Winiwarter, W., Colvile, R. N., Choularton, T. W., Flossmann, A. I., and Borrmann, S.: The Kleiner Feldberg Cloud Experiment 1990. An overview, J. Atmos. Chem., 19, 3–35, doi:10.1007/BF00696581, 1994.

Aerosol properties, source identification, and cloud processing

A. Roth et al.

Title Page

Abstract	Introduction
Conclusions	References
Tables	Figures

|◄ | ►|

◄ | ►

Back | Close

Full Screen / Esc

Printer-friendly Version

Interactive Discussion

Zelenyuk, A., Imre, D., Cai, Y., Mueller, K., Han, Y. P., and Imrich, P.: SpectraMiner, an interactive data mining and visualization software for single particle mass spectroscopy: a laboratory test case, Int. J. Mass Spectrom., 258, 58–73, doi:10.1016/j.ijms.2006.06.015, 2006.

Zelenyuk, A., Imre, D., Nam, E. J., Han, Y. P., and Mueller, K.: ClusterSculptor: software for expert-steered classification of single particle mass spectra, Int. J. Mass Spectrom., 275, 1–10, doi:10.1016/j.ijms.2008.04.033, 2008.

Zelenyuk, A., Imre, D., Earle, M., Easter, R., Korolev, A., Leaitch, R., Liu, P., Macdonald, A. M., Ovchinnikov, M., and Strapp, W.: In situ characterization of cloud condensation nuclei, interstitial, and background particles using the single particle mass spectrometer, SPLAT II, Anal. Chem., 82, 7943–7951, doi:10.1021/ac1013892, 2010.

Zhang, G. H., Bi, X. H., Chan, L. Y., Li, L., Wang, X. M., Feng, J. L., Sheng, G. Y., Fu, J. M., Li, M., and Zhou, Z.: Enhanced trimethylamine-containing particles during fog events detected by single particle aerosol mass spectrometry in urban Guangzhou, China, Atmos. Environ., 55, 121–126, doi:10.1016/j.atmosenv.2012.03.038, 2012.

Zhao, W. X., Hopke, P. K., and Prather, K. A.: Comparison of two cluster analysis methods using single particle mass spectra, Atmos. Environ., 42, 881–892, doi:10.1016/j.atmosenv.2007.10.024, 2008.

Title Page

Abstract | Introduction

Conclusions | References

Tables | Figures

◄ | ►

◄ | ►

Back | Close

Full Screen / Esc

Printer-friendly Version

Interactive Discussion

Table 1. Overview of the defined FCEs after Tilgner et al. (2014) during HCCT-2010 and the number of obtained single particle mass spectra by ALABAMA. FCE2.1, FCE4.1, FCE5.1 and FCE26.2 are statistically not significant.

Full cloud event	Start (LT)	End (LT)	Duration in h	Number of mass spectra (cloud residues)
FCE1.1	14 Sep 2010 11:00	15 Sep 2010 01:50	14.8	1351
FCE1.2	15 Sep 2010 03:00	15 Sep 2010 06:20	3.3	128
FCE2.1	15 Sep 2010 23:00	16 Sep 2010 02:00	3	–
FCE4.1	16 Sep 2010 13:10	16 Sep 2010 15:00	1.8	5
FCE5.1	16 Sep 2010 21:40	16 Sep 2010 23:50	2.2	56
FCE7.1	24 Sep 2010 21:10	25 Sep 2010 00:50	3.7	238
FCE11.2	01 Oct 2010 20:50	02 Oct 2010 03:10	6.3	117
FCE11.3	02 Oct 2010 07:10	03 Oct 2010 00:30	17.3	974
FCE13.3	06 Oct 2010 06:50	07 Oct 2010 01:00	18.2	1131
FCE22.0	19 Oct 2010 01:50	19 Oct 2010 09:00	7.2	1561
FCE22.1	19 Oct 2010 21:10	20 Oct 2010 02:30	5.3	248
FCE24.0	21 Oct 2010 22:10	22 Oct 2010 10:00	11.8	588
FCE26.1	23 Oct 2010 23:40	24 Oct 2010 07:20	7.7	356
FCE26.2	24 Oct 2010 08:40	24 Oct 2010 12:20	3.7	30

Title Page

Abstract | Introduction

Conclusions | References

Tables | Figures

◀ | ▶

◀ | ▶

Back | Close

Full Screen / Esc

Printer-friendly Version

Interactive Discussion

Table 2. Overview of particle types and the corresponding determined uncertainties of the clustering by the fuzzy c-means algorithm. The particle types "mineral dust" and "Ca" were not included in the reduced test data set.

Particle type	Number MS	$\Delta_{\text{false positive}}$	$\Delta_{\text{false negative}}$	$\Delta_{\text{particle type}}$	$\Delta_{\text{particle type}}$ (%)
org, K	274	51	43	67	24
Org	162	21	1	21	13
amines	162	14	54	56	35
Soot	125	4	19	19	15
soot and org	120	12	35	37	31
diesel exhaust	18	8	3	9	50
biomass burning	223	14	36	39	17
K	106	31	8	32	30
sea salt	23	3	5	6	26
others	164	68	22	72	44

Table 3. Overview of identified particle types and the characteristic peaks used for the assignment of clusters to a particle type. Additionally the observed chemical composition of the particle types and the denotation used in the following (legend) are listed. Secondary inorganic compounds like nitrate and sulphate were present in every particle type and have therefore not been used as characteristic signals for the separation of particle types.

Category	Legend	Method	Characteristic signals	Corresponding chemical composition
A	org, K	clustering	m/z 27 ($C_2H_3^+$), 39 (K^+), 43 ($C_3H_5^+/CH_3CO^+$), 51($C_4H_3^+$), 63 ($C_5H_3^+$),77 ($C_6H_5^+$); m/z -59 ($C_3H_7O^-/C_2H_3O_2^-$), -73 ($C_4H_9O^-/C_3H_5O_2^-$) m/z 12 (C^+),18 (NH_4^+), 27 ($C_2H_3^+$), 36 (C_3^+), 39 (K^+), 43 ($C_3H_5^+/CH_3CO^+$), 48 (C_4^+)	organics, potassium, nitrate, sulfate
B	org	clustering	m/z 27 ($C_2H_3^+$), 43 ($C_3H_5^+/CH_3CO^+$), C_{1-5}^+	organics, nitrate, sulfate
C	amines	clustering	m/z 18 (NH_4^+), 59 ($N(CH_3)_3^+$)	amines, organics, nitrate, sulfate
D	soot	clustering	C_n^+; C_n^-	soot, nitrate, sulfate
E	soot and org	clustering	m/z 18 (NH_4^+), 27 ($C_2H_3^+$) 43 ($C_3H_5^+/CH_3CO^+$), C_n^+; C_n^-	soot, organics, nitrate, sulfate
F	diesel exhaust	clustering	m/z 23 (Na^+), 40 (Ca^+), C_n^+; C_n^-	soot, sodium, calcium, nitrate
G	biomass burning	clustering	m/z 39 (K^+), C_n^+; C_n^- m/z 23 (Na^+), 39 (K^+), 43 ($C_3H_5^+/CH_3CO^+$), 51($C_4H_3^+$), C_n^+; C_n^- m/z 39 (K^+); m/z -26 (CN^-)	biomass burning, nitrate, sulfate
H	K	clustering	m/z 39 (K^+); m/z -46 (NO_2^-), -62 (NO_3^-), -97 (HSO_4^-)	potassium, nitrate, sulfate
I	sea salt	clustering	m/z 23 (Na^+), 39 (K^+); m/z -46 (NO_2^-), 62 (NO_3^-), -97 (HSO_4^-)	sodium, potassium, nitrate, sulfate (aged sea salt)
J	Ca	clustering	m/z 40 (Ca^+), 57 ($CaOH^+$)	calcium, soot, nitrate, sulfate
K	mineral dust	clustering and marker peak	m/z 56 (Fe^+)	Iron, sodium, potassium, calcium, nitrate, sulfate, phosphate
L	Fe, V	marker peak	m/z 56, m/z 51, m/z 67	vanadium, iron, nitrate, sulfate
N	Ni	marker peak	m/z 58	nickel, iron, vanadium, nitrate, sulfate
M	Pb	marker peak	m/z 208	lead, sodium, nitrate, sulfate
O	Others			

Table 4. Absolute and relative particle numbers detected by ALABAMA during the HCCT-2010 campaign. The percentage of each particle type is subdivided into the fraction revealing a diurnal trend and into the fraction without diurnal trend. All percentages refer to the total number of 177 752 analysed particles.

Particle type	Total number	Percentage	Number in clusters with diurnal trend	Percentage with diurnal trend	Number in clusters w/o diurnal trend	Percentage w/o diurnal trend
org, K	57 163	32.2	27 344	15.4	29 819	16.8
org	6295	3.54	6290	3.54	5	0.00281
amines	4910	2.76	4910	2.76	0	0
soot	25 981	14.6	23 546	13.2	2435	1.37
soot, org	3931	2.21	2878	1.62	1053	0.592
diesel exhaust	994	0.559	994	0.559	0	0
biomass burning	49 873	28.1	37 505	21.1	12 368	6.96
K	10 052	5.66	9035	5.08	1017	0.572
sea salt	1927	1.08	0	0	1927	1.08
others	13 967	7.86	0	0	13 967	7.86
Ca	263	0.148	0	0	263	0.148
mineral dust	756	0.425	0	0	756	0.425
Fe, V	569	0.242	0	0	569	0.32
Ni	641	0.361	0	0	641	0.361
Pb	430	0.242	0	0	430	0.242
Total	177 752	100	112 502	63.3	65 250	36.7

Table 5. Cloud and out-of-cloud periods (local time) used for the investigation of the particle mixing state.

Event	Out-of-cloud aerosol			Cloud residues		
	Start	End	Mass spectra	Start	End	Mass spectra
I	15 Sep 2010 11:00	15 Sep 2010 23:30	1732	14 Sep 2010 11:00	15 Sep 2010 02:00	1351
II	21 Oct 2010 14:15	21 Oct 2010 22:15	1410	21 Oct 2010 23:24	22 Oct 2010 09:29	577
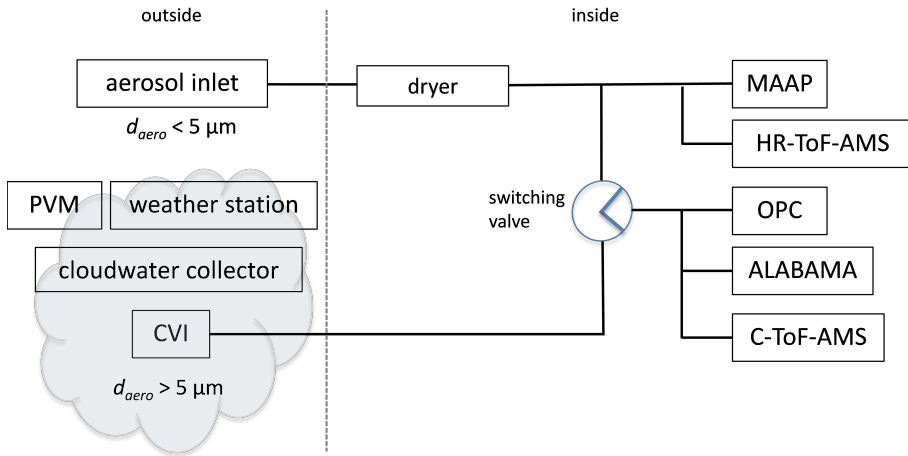
Figure 1. Measurement set-up and further operated instruments at the summit site Schmücke. Out-of-cloud aerosol was investigated by sampling through the aerosol inlet during cloud free periods while cloud residues were investigated by sampling through the CVI during cloud episodes.
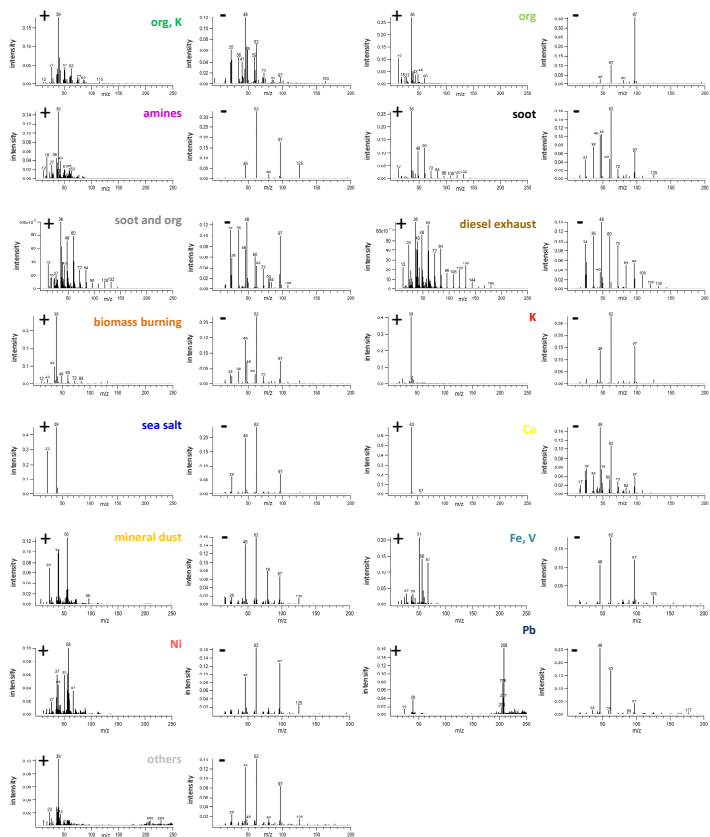
Figure 2. Mean positive (left) and negative (right) mass spectra representative of the particle types "org, K", "org", "amines", "soot", "soot and org", "diesel exhaust", "biomass burning", "K", "sea salt" and "Ca", "mineral dust", "Fe,V", "Ni", "Pb" (with the separation of the Pb isotopes clearly visible) and "others".

Title Page

Abstract | Introduction

Conclusions | References

Tables | Figures

|◄ | ►|

◄ | ►

Back | Close

Full Screen / Esc

Printer-friendly Version

Interactive Discussion
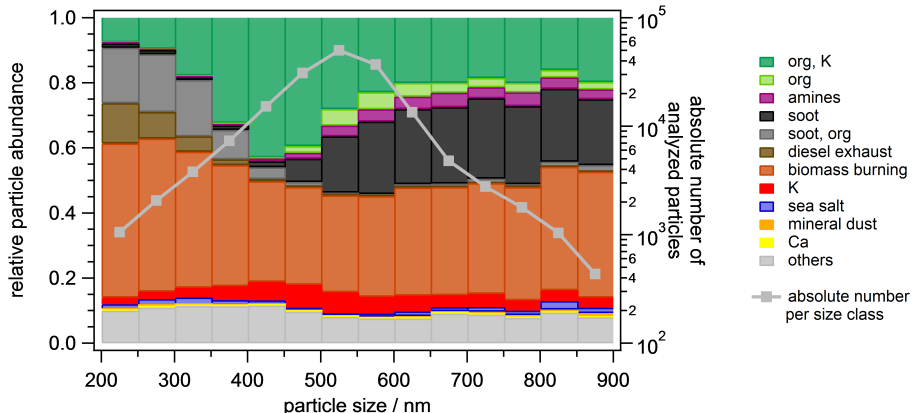
Figure 3. Size resolved aerosol composition of the resulting particle types detected by the ALABAMA, binned into 50 nm size intervals. The absolute number of analysed particles per size class is given by the grey line.
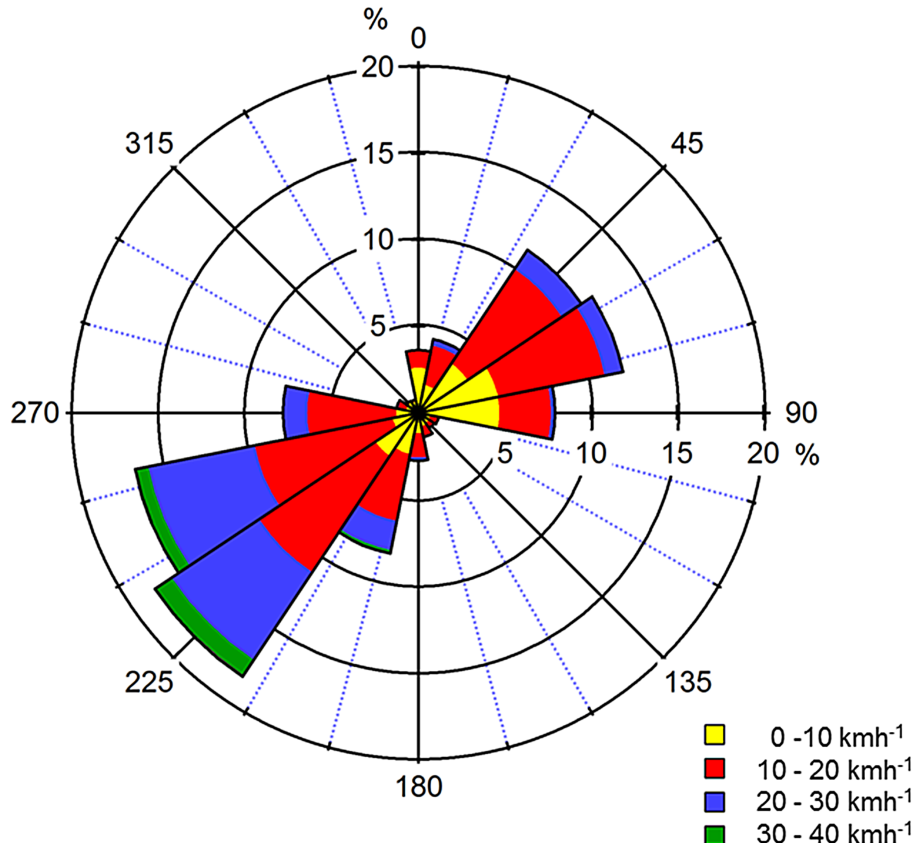
Figure 4. Occurrence of wind directions and wind velocities based on the single particle mass spectra recording time. For example, for 18 % of the detected mass spectra the wind direction was about 225°. Out of these, 10 % showed a wind velocity of 30–40 $km\,h^{-1}$, 45 % of 20–30 $km\,h^{-1}$, 40 % of 10–20 $km\,h^{-1}$ and 5 % of 0–10 $km\,h^{-1}$. The percentages of the wind velocities correspond to the coloured area fraction of the pies.
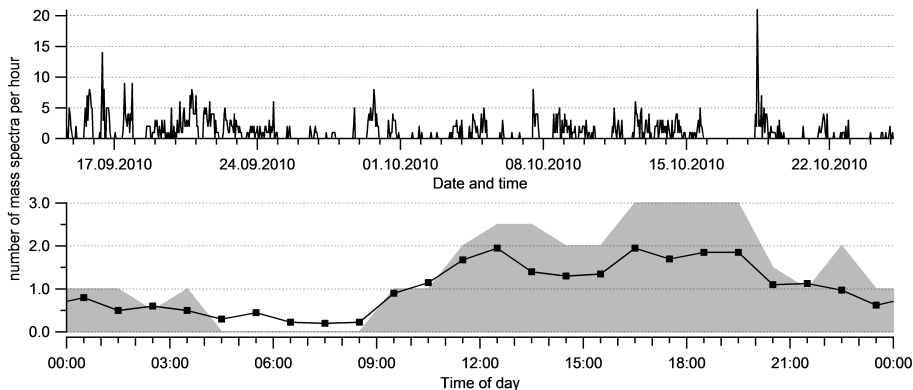
Figure 5. Time series (top) and diurnal variations (bottom, LT) of the particle type "diesel exhaust" during HCCT-2010. Markers denote the mean values, the grey shaded area represents the upper quartile.
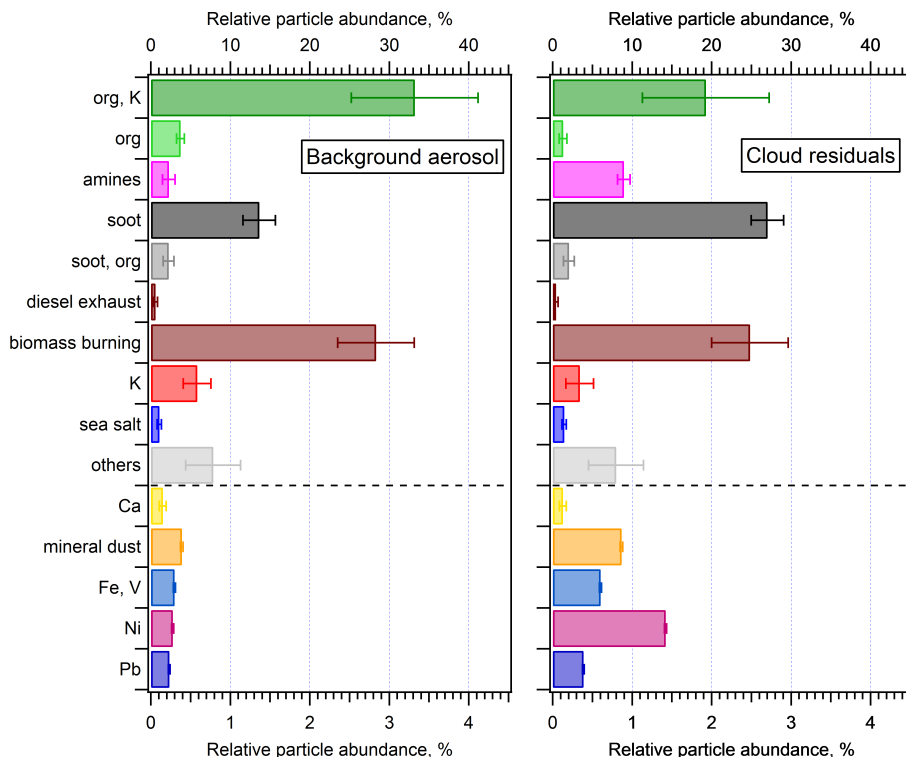
Figure 6. Aerosol composition of out-of-cloud aerosol (left) and cloud residual particles (right) for the entire HCCT-2010 campaign. Uncertainties of the clustering were estimated according to Sect. 2.4.2. In case of particle types determined by the marker peak method (Sect. 2.4.3) uncertainties are based on Poisson statistic. Number of analysed particles: out-of-cloud aerosol: 164 595, cloud residues: 13 157. Note that the scale is expanded by a factor of 10 below the dashed line (bottom axis), particle abundances above the dashed line refer to the top axis.
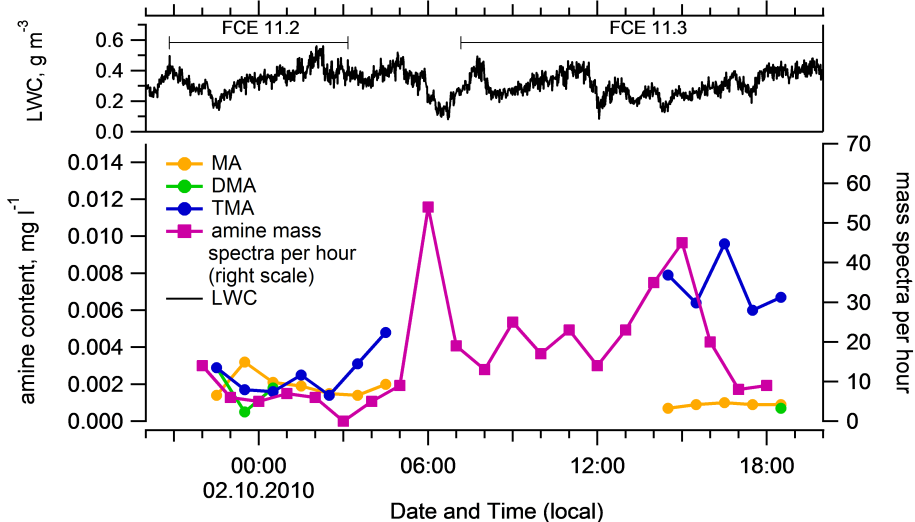
Figure 7. Time series (LT) of the amine compounds methylamine (MA), dimethylamine (DMA) and trimethylamine (TMA) from cloud water samples on 2 October 2010 (FCE11.2 and FCE 11.3) compared to the time series (number of mass spectra per hour) of amine-containing cloud residues. The upper panel shows the liquid water content (LWC) and the FCE times.
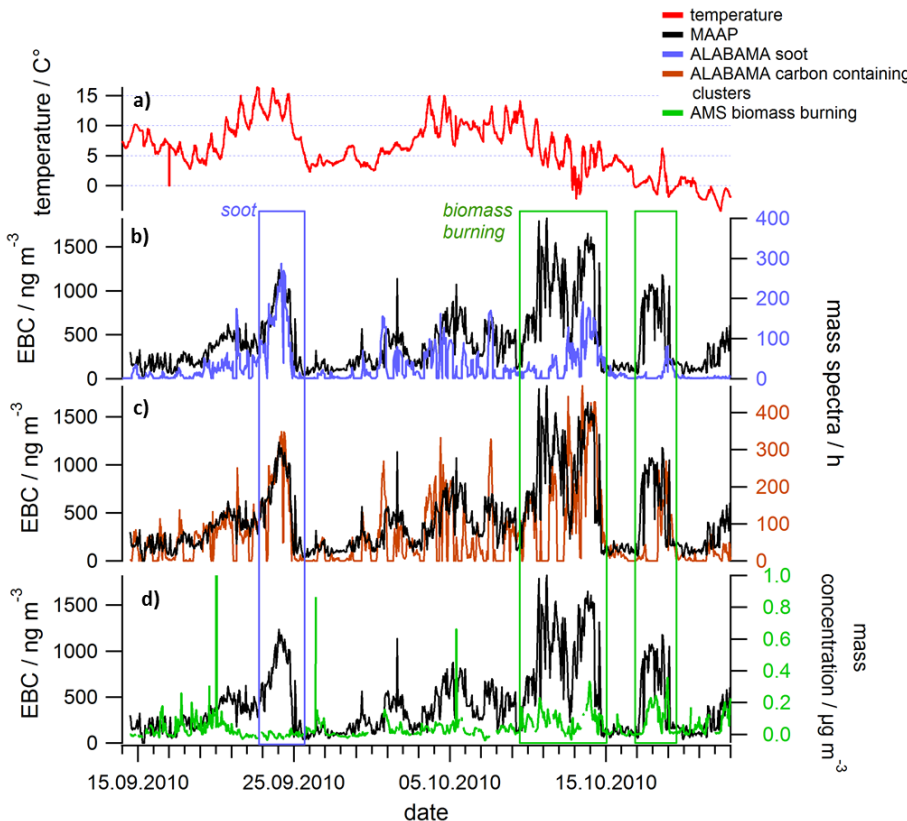
Figure 8. Time series (local time) of combustion related parameters observed during HCCT-2010. **(a)** Temperature; **(b)** Equivalent black carbon (EBC) together with the particle type "soot" (blue); **(c)** EBC along with the particle type biomass burning (brown, **(d)** EBC along with the biomass burning aerosol inferred from AMS data (green).

Title Page

Abstract | Introduction

Conclusions | References

Tables | Figures

|◄ | ►|

◄ | ►

Back | Close

Full Screen / Esc

Printer-friendly Version

Interactive Discussion
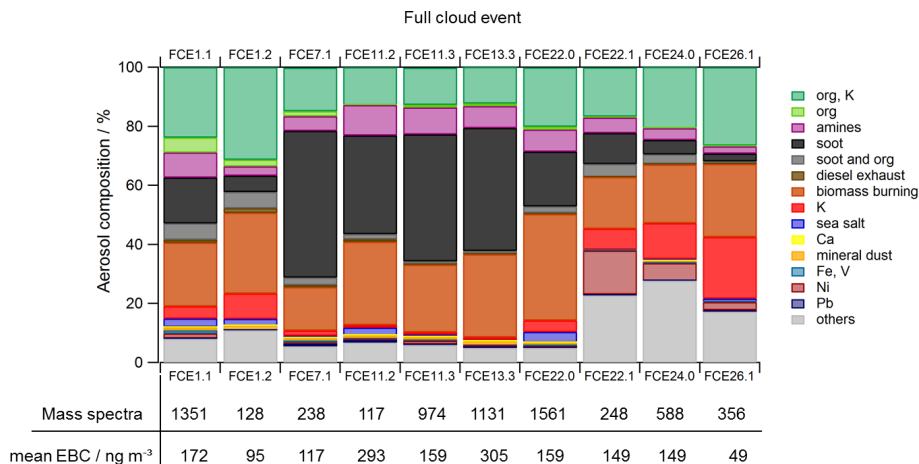
Figure 9. Cloud residue composition during full cloud events (FCE). The number of obtained single particle mass spectra and the mean EBC concentration per event is given below the graph. Only FCE with more than 100 mass spectra are included (see Table 1).
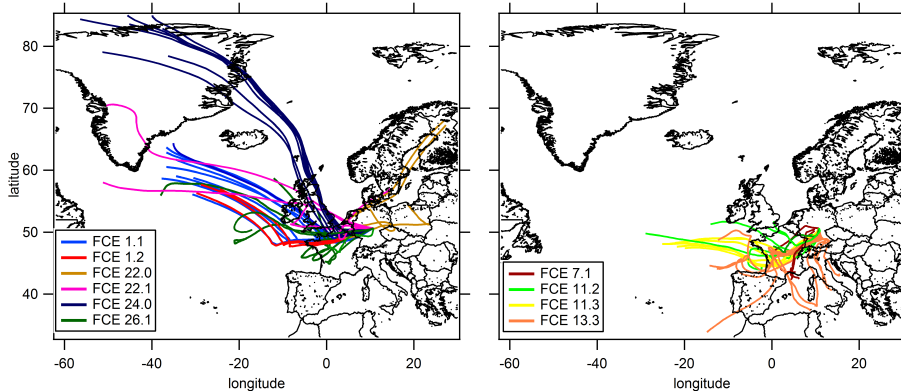
Figure 10. HYSPLIT back trajectories (96 h) for air masses encountered during the FCE displayed in Fig. 9. Left: FCE with low soot particle abundance; right: FCE with high soot particle abundance. Trajectory end point: Schmücke (10°46′15″ E, 50°39′19″ N, 500 m above model ground level). Temporal difference between successive trajectories: 2 h.
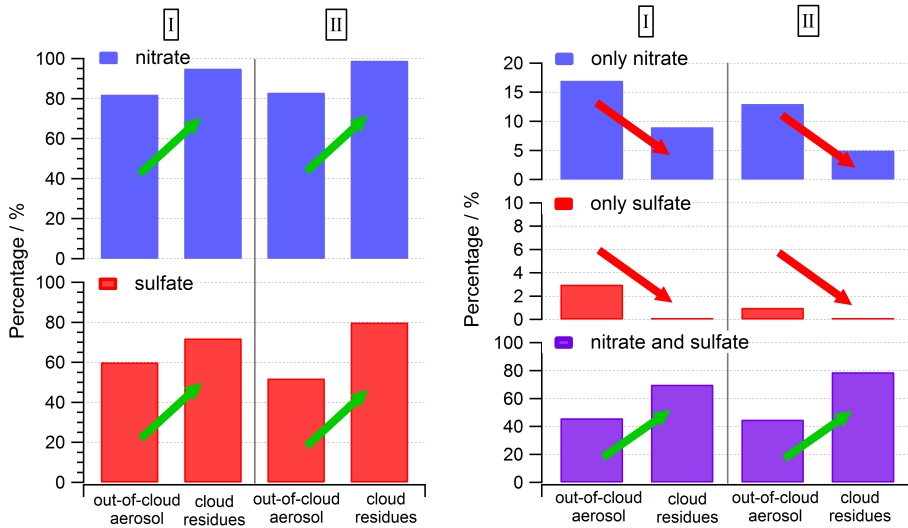
Figure 11. Indications for a change of particle mixing state in the cloud (for details of event I and II see Table 5). Left: Percentage of out-of-cloud aerosol particles and cloud residues containing either nitrate (blue) or sulphate (red). Right: Particles containing only nitrate but no sulphate (blue), only sulphate but no nitrate (red), and particles containing both nitrate and sulphate (purple).
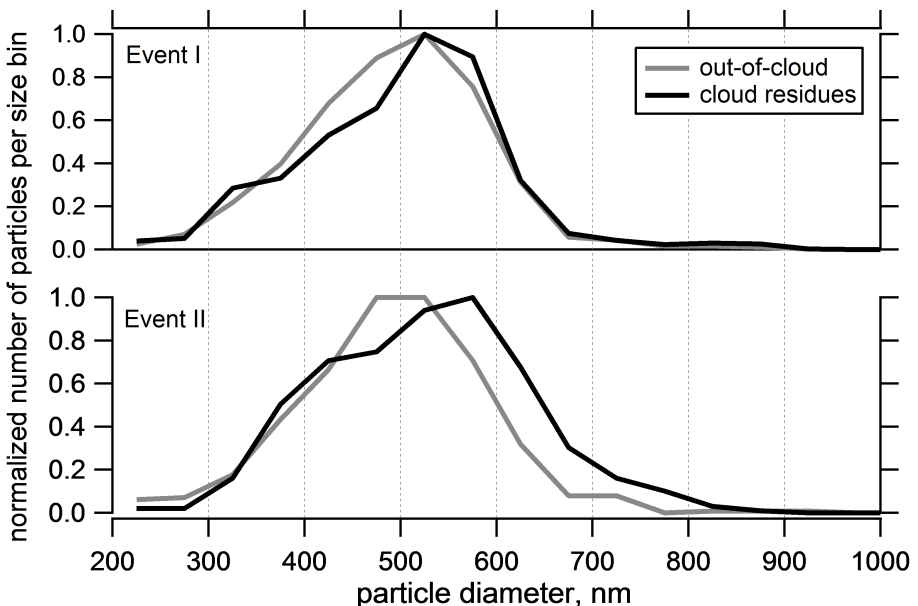
Figure 12. Histograms of particles analysed by ALABAMA during event I and event II (Table 5). In both cases the histograms are shifted to larger sizes for the cloud residues, indicating the uptake of gaseous compounds by the cloud droplets leading to an increased size of the cloud residual particles compared to the out-of-cloud particles measured shortly before cloud formation.